

# Higgs-boson visible and invisible constraints on hidden sectors

Thomas Biekötter<sup>1</sup> & Mathias Pierre<sup>2</sup>

*Deutsches Elektronen-Synchrotron DESY, Notkestr. 85, 22607 Hamburg, Germany*

## ABSTRACT

We investigate the impact of interactions between hidden sectors and the discovered Higgs boson  $h_{125}$ , allowing for additional invisible decay channels of  $h_{125}$ . We perform  $\chi^2$ -fits to the measurements of the Higgs-boson cross sections as a function of the invisible branching ratio and different combinations of coupling modifiers, where the latter quantify modifications of the couplings of  $h_{125}$  compared to the predictions of the Standard Model. We present generic results in terms of exclusion limits on the coupling modifiers and the invisible branching ratio of  $h_{125}$ . Additionally, we apply our results to a variety of concrete model realizations containing a hidden sector: dark matter within Higgs- and singlet-portal scenarios, models featuring (pseudo) Nambu-Goldstone bosons and two Higgs doublet extensions. One of the main conclusions of our work is that in a wide class of models the *indirect* constraints resulting from the measurements of the cross sections of  $h_{125}$  provide substantially stronger constraints on the invisible Higgs-boson branching ratio compared to the *direct* limits obtained from searches for the invisible decay of  $h_{125}$ . However, we demonstrate that the presence of an invisible decay mode of  $h_{125}$  can also open up parameter space regions which otherwise would be excluded as a result of the indirect constraints. As a byproduct of our analysis, we show that in light of the new results from the LZ collaboration a fermionic DM candidate within the simplest Higgs-portal scenario is ruled out under standard assumptions.

---

<sup>1</sup>thomas.biekoetter@desy.de

<sup>2</sup>mathias.pierre@desy.de

# Contents

<b>1</b>	<b>Introduction</b>	<b>1</b>
<b>2</b>	<b>Indirect limits on the invisible decay of the Higgs boson <math>h_{125}</math></b>	<b>4</b>
2.1	$h_{125}$ with SM couplings and a non-zero $\text{BR}_{\text{inv}}$ . . . . .	8
2.2	$h_{125}$ with universally modified couplings and a non-zero $\text{BR}_{\text{inv}}$ . . . . .	10
2.3	$h_{125}$ with non-universally modified couplings and a non-zero $\text{BR}_{\text{inv}}$ . . . . .	12
<b>3</b>	<b>Application to hidden sector models</b>	<b>16</b>
3.1	The Higgs portal dark matter model . . . . .	16
3.2	Singlet portal dark matter . . . . .	20
3.3	(Pseudo) Nambu-Goldstone bosons . . . . .	24
3.4	Two Higgs doublet models . . . . .	27
<b>4</b>	<b>Summary and conclusions</b>	<b>32</b>
<b>A</b>	<b>Singlet portal dark matter: additional content</b>	<b>35</b>
A.1	Minimization of the potential . . . . .	35
A.2	Decay rates . . . . .	35
	<b>References</b>	<b>36</b>

## 1 Introduction

In 2012 a particle was discovered at the Large Hadron Collider (LHC) by both the ATLAS [1] and CMS collaborations [2] with a mass of about 125 GeV that within the current experimental uncertainties behaves in agreement with the predictions for a Higgs boson of the Standard Model (SM) of particle physics [3, 4]. As a consequence, theories beyond the SM (BSM) in which the shortcomings of the SM can be addressed have to contain a particle that plays the role of the discovered Higgs boson  $h_{125}$ . This is especially relevant for BSM theories in which  $h_{125}$  is coupled to so far unknown *hidden sectors*. If the hidden sector contains particles with masses below 125 GeV, modifications of the properties of  $h_{125}$  can be present as a result of exotic decays into lighter BSM states. Here it is important to note that, in addition to the fact that the exotic decays can be searched for at colliders, additional decay modes also suppress the ordinary decay modes of  $h_{125}$  into SM particles. Therefore, the discovered Higgs boson acts as a probe for new physics beyond the SM (BSM), and the LHC plays a vital role (and will do so for many more years to come) in order to shed light on the existence of light hidden sectors that might have escaped discovery until today.

A remarkable amount of experimental knowledge about the recently discovered Higgs boson has been gathered at the LHC within the last ten years, where nature was kind to us by choosing a Higgs-boson mass for which several production modes and decay channels of  $h_{125}$  as predicted by the SM can be observed at the LHC [5]. The Higgs boson has been discovered in the gluon-fusion production mode (ggH) with subsequent decay into di-photon pairs and via its decay into pairs of

off-shell vector bosons giving rise to four-lepton final states [1, 2].<sup>3</sup> The fine mass resolution of the discovery channels permit a measurement of the mass of  $h_{125}$  at the sub-percent level [7, 8]. As of today, in addition to the ggH production mode, the production via the (tree-level) couplings to vector bosons in the vector-boson fusion (VBF) mode and via production in association with a  $W$ - or a  $Z$ -boson (VH) have been observed with a statistical significance of  $5\sigma$  or more [3, 4]. Finally, although indirect experimental evidence for the coupling of  $h_{125}$  to top-quarks was already present as a consequence of the measurement of ggH production, the presence of a large Yukawa coupling of  $h_{125}$  to top quarks has also been directly confirmed by means of the observation of Higgs-boson production in association with a top-quark pair (ttH) [3, 4]. With regards to the decays of  $h_{125}$ , in addition to the decay modes into pairs of photons and off-shell vector bosons as stated above, more recently also the decays of  $h_{125}$  into pairs of bottom quarks and into pairs of tau leptons have been observed with a statistical significance at the level of  $5\sigma$  [3, 4], such that the presence of couplings to the third-generation quarks and charged leptons has been established. Finally, there is first experimental evidence, although not yet statistically significant enough for a discovery, for the presence of rare decays of  $h_{125}$  into pairs of muons [9] and of the decays into a photon and a  $Z$ -boson [10, 11]. There is so far no statistically significant indication for exotic decay modes into hidden sectors, but the current experimental uncertainties leave room for such decays at the level of a few percent, as will be the main topic of this paper.

One of the most puzzling open problems of modern physics concerns the presence of a dark matter (DM) component in our universe, whose relative contribution to the total energy budget has been measured to a great accuracy by the Planck collaboration to be  $\Omega_{\text{DM}}h^2 = 0.11933 \pm 0.00091$  [12]. According to the standard Weakly Interacting Massive Particles (WIMP) paradigm, such a dark component could have been produced by the well-known *freeze-out* mechanism, by decoupling from the SM thermal bath while becoming non-relativistic. This scenario has been extensively studied in the literature and strong constraints from dark matter direct detection experiment, such as LUX [13], Xenon1T [14], PandaX [15] and LUX-ZEPLIN (LZ) [16], have pushed the most classic models towards corners of allowed parameter space [17–23]. The Higgs boson plays a central role in many theories attempting to solve the dark matter problem in this context as any generic theory containing a fundamental scalar could allow for this state to couple to the Higgs doublet via a quartic coupling. As the possibilities for a WIMP to carry a charge with respect to the SM gauge group are very constrained and limited [24–26], this coupling is one of the only options for a renormalizable coupling of SM singlet states to one of the SM fields, while respecting the SM gauge invariance [27]. This coupling plays a major role in the context of *Higgs portal* scenarios where a dark matter candidate interacts with the SM only via coupling to the Higgs sector [17, 20, 22, 23, 28].

Assuming, as discussed above, the presence of a hidden sector which exclusively couples to the visible sector via the Higgs portal, Higgs-boson decays into particles of the hidden sector can be kinematically allowed. Here it should be noted that one motivation to investigate hidden sectors with BSM states in this mass range is that the strongest direct detection constraints can be evaded for

---

<sup>3</sup>It is remarkable that the main discovery channel  $gg \rightarrow h_{125} \rightarrow \gamma\gamma$  involves two loop-induced processes according to the fact that the Higgs-boson does not carry color- or electric charge. As a consequence, the Higgs boson is also a valuable probe for indirect effects of BSM particles that could leave their footprint exclusively via radiative corrections to such loop-induced couplings of  $h_{125}$  (see e.g. Ref. [6]). This possibility is, however, not further considered in this paper.

Collaboration	$\sqrt{s}$ [TeV]	Data [fb $^{-1}$ ]	$h_{125}$ production	Exp. [%]	Obs. [%]
CMS [29]	8 + 13	19.7 + 140	VBF	10	<b>18*</b>
CMS [30]	7 + 8 + 13	4.9 + 19.7 + 38.2	VBF + VH + ggHj	15	<b>19</b>
CMS [31]	13	35.9	VH + ggHj	40	<b>53</b>
CMS [32]	13	35.9	ZH	44	<b>45</b>
ATLAS [33]	7 + 8 + 13	4.7 + 20.3 + 139	VBF + ttH	11	<b>11*</b>
ATLAS [34]	7 + 8 + 13	4.7 + 20.3 + 36.1	VBF + VH	17	<b>26</b>
ATLAS [35]	13	139	VBF	10.3	<b>14.5</b>
ATLAS [36]	13	36.1	ZH	39	<b>67</b>
ATLAS [37]	13	36.1	VH	58	<b>83</b>

Table 1: Expected (exp) and observed (obs) experimental upper limits at the 95% confidence level on the invisible branching ratio of  $h_{125}$  as reported by ATLAS and CMS, obtained from direct searches for the invisible decay of  $h_{125}$  at the LHC at  $\sqrt{s} = 13$  TeV. The currently strongest upper limit reported by each collaboration are marked with a star. The production modes of  $h_{125}$  targeted in the different searches are vector-boson fusion (VBF), production in association with a  $Z$ -boson (ZH) or  $Z$ - and  $W$ -bosons (VH), and gluon-fusion production in association with a jet (ggHj).

dark-matter masses at the level of a few GeV or below. If the BSM particles are stable or sufficiently long-lived in order to escape the detector, so-called invisible (inv) decays of  $h_{125}$  are present which can be searched for at the LHC in final states with large missing transverse energy. Direct searches for the invisible decay of  $h_{125}$  have been performed by both the ATLAS and the CMS collaboration utilizing various different production modes. We summarize in Tab. 1 the current LHC searches for the invisible decay of  $h_{125}$  that include part or all of the Run 2 dataset at 13 TeV. No significant excesses over the SM background have been observed, such that upper limits on the branching ratio for the invisible decay of  $h_{125}$ , denoted  $\text{BR}_{\text{inv}}$  from hereon, have been determined (see last column of Tab. 1). Assuming that  $h_{125}$  couples to the SM fermions and gauge bosons according to the predictions of the SM, the currently strongest limit on  $\text{BR}_{\text{inv}}$  was reported by ATLAS [33],

$$\text{BR}_{\text{inv}} < 11\% \quad \text{at 95\% confidence level (CL)}, \quad (1.1)$$

which was obtained by combining the datasets collected at 7, 8 and 13 TeV, and by utilizing the VBF and ttH production modes. In the following, we will refer to the constraint shown in Eq. (1.1) as the *direct limit* on  $\text{BR}_{\text{inv}}$ , according to the fact that it is extracted from directly searching for the invisible decay of  $h_{125}$ .

In many phenomenological analyses of BSM theories in which a Higgs-boson invisible decay plays a role, only the above mentioned direct limit on  $\text{BR}_{\text{inv}}$  is applied in order to exclude parameter space regions of the theory that are in disagreement with the Higgs-boson measurements at the LHC (see e.g. Refs. [17, 19, 21, 38–40]). However, additional, although more model-dependent, constraints on  $\text{BR}_{\text{inv}}$  arise from the cross-section measurements of  $h_{125}$ , considering that additional BSM decay modes give rise to a suppression of the ordinary decay modes of  $h_{125}$ . By performing global scans to the LHC Higgs-boson measurements in terms of  $\text{BR}_{\text{inv}}$  and so-called coupling modifiers that quantify deviations of the couplings of  $h_{125}$  with respect to the SM predictions, one can set limits on  $\text{BR}_{\text{inv}}$  as a function of the coupling modifiers (see, e.g. Refs. [41–46] for earlier analyses of this kind). Since in this approach the measurements of the ordinary decay modes of  $h_{125}$  are used to constrain  $\text{BR}_{\text{inv}}$ ,

in contrast to directly searching for the invisible decay of  $h_{125}$ , we will refer to the limits on  $\text{BR}_{\text{inv}}$  resulting from the global analysis of the cross-section measurements as the *indirect constraints* in the following.

In this paper our goal is to exploit the complementarity of the direct and the indirect constraints on  $\text{BR}_{\text{inv}}$ . To this end, the first step of our analysis is to determine the indirect constraints on  $\text{BR}_{\text{inv}}$  via global fits to the cross-section measurements of  $h_{125}$ , where we will make use of the public code `HiggsSignals v.3` [47]. We perform such global scans assuming that the couplings of  $h_{125}$  remain unchanged compared to the couplings of a SM Higgs boson, but also assuming more complicated Higgs-portal models in which, in addition to the presence of an invisible decay mode, there are modifications of the couplings of  $h_{125}$  to the fermions and gauge bosons.<sup>4</sup> If coupling modifications are considered, the upper limit on  $\text{BR}_{\text{inv}}$  is a function of the coupling modifiers. Having determined the indirect constraints on  $\text{BR}_{\text{inv}}$ , we then compare them to the direct limit on  $\text{BR}_{\text{inv}}$  in order to investigate which of the two kind of constraints results in a stronger exclusion in a variety of different BSM scenarios. To give a brief outlook on the key results that we have found, we emphasize already here that in many of the Higgs-portal scenarios considered in the literature the indirect constraints can provide substantially stronger exclusions and should therefore not be overlooked. However, in models in which the properties of  $h_{125}$  are not as predicted by the SM, we also found parameter space regions that are in conflict with the LHC Higgs-boson measurements if there is no invisible decay mode of  $h_{125}$ , whereas the same parameter regions are well in agreement with the LHC measurements if a value of  $\text{BR}_{\text{inv}}$  at the level of a few percent is present.

The outline of the paper is as follow. In Sec. 2 we describe the setup and approach used to derive the indirect constraints on  $\text{BR}_{\text{inv}}$  as a function of the couplings modifiers, thus accounting for deviations with respect to the SM expectation of the couplings of  $h_{125}$  to the SM fields. We present generic constraints in terms of the coupling modifiers and the invisible branching fraction for a different set of assumption regarding the structure of the coupling modifiers. Going beyond this generic framework, we analyse in Sec. 3 the constraints in a variety of concrete BSM scenarios: Higgs- and singlet-mediated dark matter models, constructions featuring (pseudo) Nambu-Goldstone bosons, and extended Higgs sectors featuring a second Higgs doublet. In Sec. 4, we summarize our main results and conclude.

## 2 Indirect limits on the invisible decay of the Higgs boson $h_{125}$

As mentioned above, in the first step of our analysis we will remain agnostic about the precise nature of the hidden sector. Instead of specifying a concrete model, we perform  $\chi^2$ -fits to the measurements of the Higgs boson  $h_{125}$  as a function of the branching ratio for invisible decay modes of  $h_{125}$  and, in addition, as a function of coupling modifiers that quantify modifications of the couplings of  $h_{125}$  compared to the SM predictions. These  $\chi^2$ -analyses, for which we make use of the public code `HiggsSignals v.3` [46, 47, 50] (see the discussion below for details), will be discussed in this section. The  $\chi^2$ -analyses provide us with 68% and 95% confidence-level (CL) upper limits on  $\text{BR}_{\text{inv}}$  as a function of the coupling modifiers. These upper limits can be compared to the upper limits on the invisible branching ratio resulting from direct-searches for the decays of  $h_{125}$  into invisible

---

<sup>4</sup>Similar analyses have been performed, for instance, in Refs. [42, 46, 48, 49], and more recently both CMS and ATLAS presented constraints on  $\text{BR}_{\text{inv}}$  obtained in the so-called  $\kappa$ -framework [3, 4].

final state. At a later stage of our analysis, discussed in Sec. 3, we will apply the constraints on the invisible branching ratio  $\text{BR}_{\text{inv}}$  that we obtained from the global  $\chi^2$ -fit to a range of commonly studied hidden sectors possessing dark matter candidates, extended scalar content (2HDM) and pseudo Nambu-Goldstone bosons, in which the Higgs portal plays a major role.

Before starting the discussion of the results of the  $\chi^2$ -analyses, we briefly discuss the strategy that is implemented in the public code `HiggsSignals`, and which is used here in order to compare the predicted cross sections and signal rates of  $h_{125}$  to the experimental measurements. For a more detailed description of the code, we refer the reader to Ref. [47] (see also Ref. [46] for a more detailed discussion on the statistical interpretation of the  $\chi^2$ -values provided by `HiggsSignals`). The code contains a large set of experimental data from LHC measurements at 8 TeV and (mostly) 13 TeV center-of-mass energy.<sup>5</sup> The measurements are implemented not only in the form of inclusive cross sections (or signal rates), but also in the form of the simplified template cross sections [51] which were designed to allow for a combination of measurements of different decay channels of  $h_{125}$ . In total, the `HiggsSignals` dataset currently comprises 24 independent measurements from the CMS and the ATLAS collaborations. For the purpose of our paper, as will be discussed in detail below, the most important measurements are the ones utilizing the di-photon final state due to the sensitivity of the di-photon branching ratio on the presence of BSM decay modes of  $h_{125}$ .

On the theory side, in order to compare the model predictions to the experimental data, `HiggsSignals` requires as input either directly the signal rates (or alternatively the cross sections and branching ratios) of  $h_{125}$  in the various different production or decay modes, or the user has the option to provide effective coupling modifiers from which the cross sections and branching ratios are derived internally by a re-scaling of the SM predictions. The coupling modifiers are defined as the couplings of the particle state at 125 GeV in the given BSM theory normalized to the couplings of a SM Higgs boson at the same mass (see below for details). Thus, in order to check the SM against the experimental data, one would choose all modifiers to be equal to one, whereas in models that feature modifications of the properties of  $h_{125}$  the couplings modifiers deviate from one. In our analysis, we will combine both input formats. This is possible since the most recent update of `HiggsSignals`, which is now incorporated into the public code `HiggsTools` [47]. We make use of the input in terms of the coupling modifiers in order to obtain the LHC cross sections of  $h_{125}$  and in order to calculate the partial decay widths of all conventional decay modes of  $h_{125}$  into SM particles. Subsequently, in order to set the desired value of the branching ratio for the additional decay mode into invisible final states, we give the respective partial decay width  $\Gamma_{\text{inv}}$  as input. The partial width  $\Gamma_{\text{inv}}$  that is required to set a desired value of  $\text{BR}_{\text{inv}}$  can be calculated as

$$\Gamma_{\text{inv}} = \frac{\text{BR}_{\text{inv}}}{1 - \text{BR}_{\text{inv}}} \sum_i \Gamma_i^{\text{SM}}, \quad (2.1)$$

where  $\Gamma_i^{\text{SM}}$  stands for the individual partial widths for decays of  $h_{125}$  into SM final states, which were calculated previously as a function of the coupling modifiers. Accordingly, the sum runs over all relevant SM decay modes of  $h_{125}$ , i.e.  $i = \{b\bar{b}, gg, WW^*, ZZ^*, c\bar{c}, s\bar{s}, \tau^+\tau^-, \gamma\gamma, \mu^+\mu^-, Z\gamma\}$ . The total width of  $h_{125}$  is then given by

$$\Gamma_{\text{tot}} = \Gamma_{\text{inv}} + \sum_i \Gamma_i^{\text{SM}}. \quad (2.2)$$

---

<sup>5</sup>The data repository of `HiggsSignals` can be found at <https://gitlab.com/higgsbounds/hsdataset>.

Scenario	$c_u$	$c_d$	$c_\ell$	$c_V$	Discussion
SM-like couplings	1	1	1	1	Sec. 2.1
Universal couplings	$c_{\text{uni}}$	$c_{\text{uni}}$	$c_{\text{uni}}$	$c_{\text{uni}}$	Sec. 2.2
Non-universal couplings	$c_f$	$c_f$	$c_f$	$c_V$	Sec. 2.3
Non-universal couplings	$c_u$	$c_d$	$c_\ell = c_d$	1	Sec. 2.3
Higgs portal DM	1	1	1	1	Sec. 3.1
Singlet portal DM	$c_{\text{uni}} \leq 1$	$c_{\text{uni}} \leq 1$	$c_{\text{uni}} \leq 1$	$c_{\text{uni}} \leq 1$	Sec. 3.2
(P)NGB	$c_{\text{uni}} \leq 1$	$c_{\text{uni}} \leq 1$	$c_{\text{uni}} \leq 1$	$c_{\text{uni}} \leq 1$	Sec. 3.3
2HDM Type I	$c_f$	$c_f$	$c_f$	$c_V \leq 1$	Sec. 3.4
2HDM Type II	$c_u$	$c_d$	$c_\ell = c_d$	$c_V \leq 1$	Sec. 3.4
2HDM Type III	$c_u$	$c_d = c_u$	$c_\ell = c_u$	$c_V \leq 1$	Sec. 3.4
2HDM Type IV	$c_u$	$c_d$	$c_\ell = c_u$	$c_V \leq 1$	Sec. 3.4

Table 2: Summary of the coupling modifications in terms of the modifiers defined in Eq. (2.3) for the various models considered in this work and references to the (sub)sections of the manuscript where each specific case is discussed.

As already discussed in the introduction, the fact that the total width of  $h_{125}$  is modified via the presence of the additional contribution  $\Gamma_{\text{inv}}$  gives rise to the fact that  $\text{BR}_{\text{inv}}$  can be constrained via the measured cross sections and signal rates of  $h_{125}$ .

In order to capture the coupling modifications that arise in as many UV-complete models as possible while maintaining a manageable number of free parameters, we define four independent coupling modifiers  $c_i$ , with  $i = V, u, d, \ell$ . The coefficients  $c_i$  modify the couplings of the discovered Higgs boson  $h_{125}$  to the SM mass eigenstates according to

$$\mathcal{L} = \sum_{f=u,d,\ell} c_f \left( \frac{m_f}{v} \right) h_{125} \bar{f}f + c_V \left( \frac{2m_W^2}{v} \right) h_{125} W^{+\mu}W_\mu^- + c_V \left( \frac{m_Z^2}{v} \right) h_{125} Z^\mu Z_\mu + \mathcal{L}_{\text{inv}}, \quad (2.3)$$

where  $c_V$ ,  $c_u$ ,  $c_d$  and  $c_\ell$  are, respectively, the coupling modifier of the massive gauge bosons, to up-type quarks, to down-type quarks and charged leptons.<sup>6</sup>  $\mathcal{L}_{\text{inv}}$  is the contribution that contains the portal couplings to the hidden sector responsible for the presence of the invisible branching ratio  $\text{BR}_{\text{inv}}$ , which we will further specify when we consider concrete BSM theories in Sec. 3. For the loop-induced couplings of  $h_{125}$  to photons and gluons, we assume that there are no sizable BSM contributions in additions to the loop diagrams with SM particles in the loops, reflecting the fact that light hidden-sector particles can only couple very weakly via the SM gauge interactions in order to be physically viable. Hence, the respective coupling coefficients  $c_{\gamma\gamma}$  and  $c_{gg}$  can be calculated as a function of  $c_V$ ,  $c_u$  and  $c_d$ .<sup>7</sup> The structure of the coupling modifiers in the various BSM theories considered in this work are summarized in Tab. 2.

As already mentioned above, in order to derive the indirect limits on  $\text{BR}_{\text{inv}}$  from the measurements related to  $h_{125}$  we perform a  $\chi^2$ -analysis utilizing the public code **HiggsSignals**. We determine in

<sup>6</sup>Consequently, we do not take into account flavour-dependent modifications to the Higgs-boson couplings. We also do not consider possible sources of CP violation, such that  $h_{125}$  is assumed to be a purely CP-even state.

<sup>7</sup>The contributions from the charged leptons can safely be neglected due to the suppression from the smaller Yukawa couplings  $Y_\ell \ll Y_t, Y_b$ .

each scan

$$\Delta\chi^2(c_i, \text{BR}_{\text{inv}}) = \chi^2(c_i, \text{BR}_{\text{inv}}) - \chi_{\text{SM}}^2, \quad (2.4)$$

where  $\chi^2(c_i, \text{BR}_{\text{inv}})$  is the fit result for the respective BSM scenario given as a function of the coupling modifiers  $c_i$  and  $\text{BR}_{\text{inv}}$ , and  $\chi_{\text{SM}}^2$  is the fit result assuming properties of  $h_{125}$  as predicted by the SM, i.e.  $\text{BR}_{\text{inv}} = 0$  and  $c_i = 1$ .<sup>8</sup> In order to set limits on the coupling modifiers or model parameters, we demand that the BSM scenario is not disfavoured compared to the SM fit result at the 95% CL or more. In a one-dimensional parameter estimation, this translates into the condition [53]

$$\Delta\chi^2 \leq 3.84. \quad (2.5)$$

In a joint estimation of two free parameters, the respective condition is

$$\Delta\chi^2 \leq 5.99. \quad (2.6)$$

In addition to the allowed regions of the coupling modifiers obtained using the 95% CL conditions, we will show in our plots also allowed regions using the 68% ( $1\sigma$ ) CL for illustrative reasons, which corresponds to the conditions  $\Delta\chi^2 \leq 1$  and  $\Delta\chi^2 \leq 2.30$  in one-dimensional and two-dimensional fits, respectively [53].

By defining the allowed/excluded regions for the coupling modifiers based on the  $\chi^2$ -definition shown in Eq. (2.4), where we utilize the SM as a reference model, the obtained limits only correspond to the 95% CL limits if the SM result  $\chi_{\text{SM}}^2$  is a good approximation of the best-fit result of the BSM scenario under consideration, i.e.  $\chi_{\text{min}}^2 = \min(\chi^2) \simeq \chi_{\text{SM}}^2$ . As we will discuss below, we encountered situations in which  $\chi_{\text{min}}^2$  was considerably smaller than  $\chi_{\text{SM}}^2$  for certain parameter configurations.<sup>9</sup> In such a situation, the more common approach (in a frequentist analysis) would be to construct the confidence intervals of the free parameters by comparing to the parameter point that features the best-fit value  $\chi_{\text{min}}^2$  instead of comparing to  $\chi_{\text{SM}}^2 > \chi_{\text{min}}^2$ , i.e. constructing the limits based on  $\Delta\chi^2 = \chi^2 - \chi_{\text{min}}^2$ . This approach would yield stronger constraints on the parameters and therefore smaller allowed regions in the  $c_i$  parameter space as compared to our approach, such that the latter should be regarded as more conservative. We found that the experimental measurements responsible for values of  $\Delta\chi^2 < 0$  are mainly the ones related to the ttH production of  $h_{125}$ , where the signal extraction is affected by systematic uncertainties regarding the theoretical predictions for the background estimation [54, 55]. Taking this into account, it is reasonable to be conservative in the determination of the exclusion limits, thus sticking to the definition of  $\Delta\chi^2$  as shown in Eq. (2.4), even though  $\chi_{\text{min}}^2$  is smaller than  $\chi_{\text{SM}}^2$  in some scenarios. We also note that in our plots we indicate the  $\Delta\chi^2$ -distribution together with the value of  $\chi_{\text{min}}^2$  for all parameter points in addition to the 68% CL and 95% CL exclusions, such that the reader can also apply a different criterion in order to define the allowed regions. Finally, it should also be noted that the opposite case with  $\chi_{\text{min}}^2 > \chi_{\text{SM}}^2$

---

<sup>8</sup>Strictly speaking, also in the SM one finds  $\text{BR}_{\text{inv}} > 0$  due to the decay mode  $h_{125} \rightarrow ZZ^* \rightarrow \nu\nu\bar{\nu}\bar{\nu}$ . However, the resulting branching ratio is of the order of 0.1% [52]. Considering the current experimental precisions of the signal-rate measurements of  $h_{125}$ , this value can be approximated by zero for all practical purposes.

<sup>9</sup>We emphasize that  $\chi_{\text{min}}^2 < \chi_{\text{SM}}^2$  does not necessarily signify a global statistical preference of the respective BSM scenario compared to the SM, as such a conclusion can only be drawn by also taking into account the different numbers of degrees of freedom of both models. For the context of our analysis, in which we are interested only in the constraints on the coupling modifiers and  $\text{BR}_{\text{inv}}$  that can be derived within a certain BSM scenario, the global preference of different BSM scenarios against the SM (and also against each other) is not relevant.



is not possible for the different BSM scenarios considered in the following, because in the fits of the BSM theories in terms of the coupling modifiers we always include the parameter space point  $c_i = 1$  and  $\text{BR}_{\text{inv}} = 0$  in which the particle state  $h_{125}$  resembles exactly the properties of a SM Higgs boson.

As was already mentioned above, we start our analysis by performing the  $\chi^2$ -fits in different BSM scenarios in a generic fashion in terms of the coupling modifiers  $c_i$ . The different scenarios are discussed in the following subsections. We summarize in Tab. 2 the different constructions of coupling modifications that we consider. The applications of the constraints on the modifiers  $c_i$  and ultimately on  $\text{BR}_{\text{inv}}$  obtained in this way to the parameter space of UV-complete BSM theories, in which both  $c_i$  and  $\text{BR}_{\text{inv}}$  are functions of the model parameters, will be discussed in Sec. 3.

## 2.1 $h_{125}$ with SM couplings and a non-zero $\text{BR}_{\text{inv}}$

In the simplest hidden sector models, the SM is augmented by new fields which do not give rise to modifications of the couplings of  $h_{125}$  compared to a SM Higgs boson. As a result, the cross sections at colliders for the production of  $h_{125}$  are unchanged compared to the SM predictions. However, as discussed above, the branching ratios of  $h_{125}$  can be modified due to additional decay modes into the hidden sector if such decay modes are kinematically allowed. In this case, the modifications of the properties of  $h_{125}$  compared to the SM predictions can be quantified exclusively in terms of the invisible branching ratio  $\text{BR}_{\text{inv}}$ . In the following we will discuss how non-zero values of  $\text{BR}_{\text{inv}}$  give rise to a suppression of the signal rates in the conventional decay modes of  $h_{125}$ . By comparing the predicted signal rates to the experimental measurements, we will derive an upper limit on  $\text{BR}_{\text{inv}}$  at the 95% CL via the condition shown in Eq. (2.5). Finally, we will compare the indirect limit resulting from the global Higgs-boson measurements to the direct limit on  $\text{BR}_{\text{inv}}$  from direct searches for the invisible decay of  $h_{125}$ .

To this end, we show in Fig. 1 the results of the  $\chi^2$ -analysis performed with `HiggsSignals`, where we set  $c_i = 0$ , and we varied  $\text{BR}_{\text{inv}}$  from 0% to 18%. The black solid line indicates the value of  $\Delta\chi^2$ , which is obtained including the complete data set implemented in `HiggsSignals`. We find the best-fit with  $\Delta\chi^2 = 0$  at  $\text{BR}_{\text{inv}} = 0$ , with  $\chi_{\text{min}}^2 = \chi_{\text{SM}}^2 = 151.67$ . For increasing values of  $\text{BR}_{\text{inv}}$  the  $\chi^2$  function is monotonically increasing. Consequently, under the assumption that the couplings of  $h_{125}$  are unchanged compared to the SM predictions, the presence of an invisible decay mode of  $h_{125}$  with sizable branching ratio worsens the fit result to the Higgs-boson measurements for all possible values of  $\text{BR}_{\text{inv}}$ . Based on the `HiggsSignals` analysis, we find an indirect upper limit of

$$\text{BR}_{\text{inv}} < 6.22\% \text{ (3.08\%)} \quad \text{at 95\% (68\%) CL} \quad \text{for } c_i = 1 . \quad (2.7)$$

The 95% CL limit is almost a factor of two smaller than the currently strongest limits from direct searches for the decay mode  $h_{125} \rightarrow \text{inv}$  (see Tab. 1). The strongest direct limit  $\text{BR}_{\text{inv}} < 11\%$  is indicated by the orange dotted-dashed vertical line in Fig. 1 [33]. Accordingly, for phenomenological studies of models with hidden sectors in which the couplings of  $h_{125}$  are not modified compared to the SM predictions, but where the decay of  $h_{125}$  into the hidden sector is kinematically open, one should include the indirect constraints from the measurements of the signal rates of  $h_{125}$ , currently giving rise to the upper limit shown in Eq. (2.7). On the contrary, taking into account only the limit on  $\text{BR}_{\text{inv}}$  from direct searches allows also parameter space regions that are already excluded by the measurements regarding the discovered Higgs boson at a CL of more than  $3\sigma$ , i.e.  $\Delta\chi^2 > 9$ , as is visible in Fig. 1.

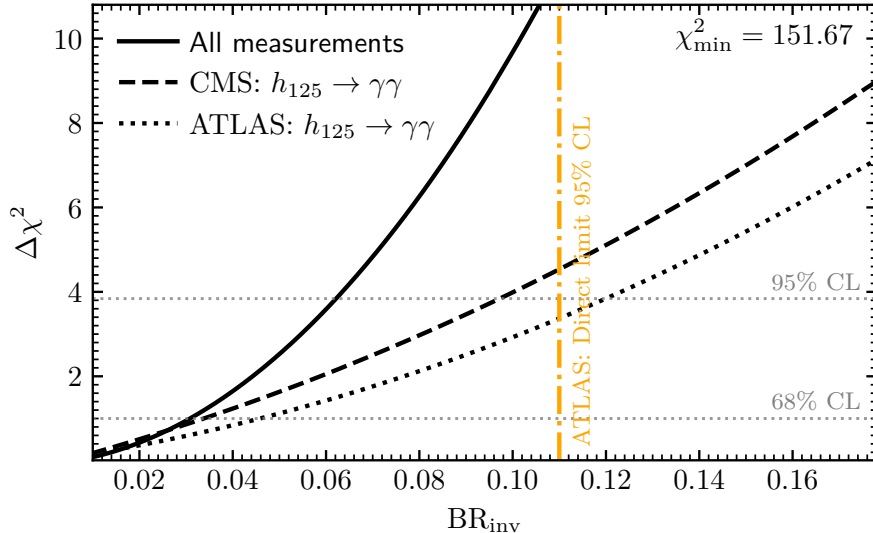


Figure 1: Result of the global fit to the Higgs signal-rate measurements assuming a Higgs boson  $h_{125}$  that apart from the presence of an invisible decay mode behaves according to the predictions of the SM model, i.e. the couplings of  $h_{125}$  to the SM particles are unchanged. The black solid line indicates the value  $\Delta\chi^2$  taking into account the full `HiggsSignals` data set. The black dashed and the black dotted lines indicate the value of  $\Delta\chi^2$  considering only the measurements in the diphoton final state utilizing the full Run 2 data by CMS [56] and ATLAS [57], respectively. The gray horizontal lines indicate the 68% and 95% CL, respectively. The orange vertical line indicates the currently strongest upper limit on  $\text{BR}_{\text{inv}}$  resulting from direct searches for  $h_{125} \rightarrow \text{inv}$  as published by ATLAS [33].

In order to shed light on which particular measurements are most relevant for the increase of  $\chi^2$  with increasing values of  $\text{BR}_{\text{inv}}$ , we show in Fig. 1 the  $\chi^2$ -values that are obtained only taking into account the measurement with the largest and the second largest individual contributions to the total  $\chi^2$ .<sup>10</sup> The most important  $\chi^2$ -penalty has its origin in the CMS measurement of Higgs-boson production and subsequent decay into di-photon pairs including the full Run 2 data at 13 TeV center of mass energy [56]. The fit to the corresponding cross-section measurements gives rise to the  $\Delta\chi^2$  values indicated by the black dashed line in Fig. 1. One can see that based on this measurement alone one obtains a stronger upper limit on  $\text{BR}_{\text{inv}}$  than the one obtained from direct searches for  $h_{125} \rightarrow \text{inv}$ . Also the second largest  $\chi^2$ -penalty is caused by signal rates of  $h_{125}$  utilizing the diphoton decay mode, but here as a result of the corresponding ATLAS measurements [57], indicated by the black dotted line in Fig. 1. The fact that the two most relevant measurements are both related to the  $h_{125} \rightarrow \gamma\gamma$  decay mode can be understood by realizing that, from the experimental side, it is the most precisely measured decay mode, and that, from the theory side, the di-photon branching ratio is very sensitive to modifications of the total width of  $h_{125}$ .

We finally compare the indirect limit on  $\text{BR}_{\text{inv}}$  to similar results that have been obtained in the past and to projections for future runs of the LHC and for the high-luminosity LHC (HL-LHC). An early analysis including Tevatron and LHC first-year Run 1 data found a limit of  $\text{BR}_{\text{inv}} \leq 23\%$  via a

<sup>10</sup>The total  $\chi^2$ -value including all measurements (black solid line) can be smaller than the sum of the two individual contributions from the  $h_{125} \rightarrow \gamma\gamma$  measurements (black dashed and dotted lines) shown in Fig. 1, because for the computation of the total  $\chi^2$ -values the correlations are taken into account.

global fit to the Higgs-boson data assuming SM-like couplings [43]. Shortly after, in Ref. [44] a slightly stronger limit of  $\text{BR}_{\text{inv}} \leq 17\%$  was found making use of `HiggsSignals` using the same fit strategy as applied here. Taking into account the full Run 1 LHC data, an upper limit of  $\text{BR}_{\text{inv}} \leq 12\%$  has been determined in Ref. [49]. Global fits including also 13 TeV LHC data have been performed in Ref. [45] and Ref. [46], finding upper limits on  $\text{BR}_{\text{inv}}$  under the assumption of SM-like couplings of 5% and 10%, respectively. These numbers are of comparable size as the limit  $\text{BR}_{\text{inv}} \leq 6.2\%$  found in this analysis.

It is interesting to note that the current indirect limits are also comparable to the HL-LHC projections assuming that  $3000 \text{ fb}^{-1}$  will be collected at 14 TeV [58]. The reason for this is mainly that the projected limits on  $\text{BR}_{\text{inv}}$  were obtained under the assumptions that the experimental data will be in agreement with the SM predictions, whereas the current limits on  $\text{BR}_{\text{inv}}$  have been determined from actual data in which the central values of the various measurements naturally fluctuate within statistical and systematic uncertainties. If differences exist between the central values in the current data and the SM predictions (which are expected at least at the level of statistical fluctuations), the extracted upper limit on  $\text{BR}_{\text{inv}}$  derived today can be smaller than the projected HL-LHC limit even though the precision of the individual cross-section measurements is larger now compared to what is expected in the future for the HL-LHC. This also means that, even though the uncertainties of the cross-section measurements of  $h_{125}$  will improve in the future, the indirect limit on  $\text{BR}_{\text{inv}}$  might not necessarily become substantially stronger, because the limit will depend on how the measured central values of the cross sections will evolve within the current uncertainty bands.

## 2.2 $h_{125}$ with universally modified couplings and a non-zero $\text{BR}_{\text{inv}}$

In the previous section we discussed the case in which the Higgs sector remained unchanged compared to the SM except for the presence of an additional invisible decay mode into a hidden sector. However, in many BSM scenarios additional scalar fields can mix with the SM-like Higgs boson at 125 GeV. In this case, the properties of  $h_{125}$  can be modified not only by additional decay modes into invisible final states, but also the couplings of  $h_{125}$  to the fermions and gauge bosons of the SM can be modified compared to the SM. In this section we will analyze the most simple possibility, in which the couplings of  $h_{125}$  to the SM particles are modified by a universal coupling modifier  $c_{\text{uni}} = c_V = c_u = c_d = c_\ell$ . The simplest UV-complete model in which this pattern of coupling modifiers arises is a model in which a gauge singlet scalar field mixes with  $h_{125}$ , giving rise to a suppression of the couplings of  $h_{125}$  by a universal factor  $c_{\text{uni}} < 1$  which can be identified as  $c_{\text{uni}} = \cos \theta$  where  $\theta$  is the singlet mixing angle with  $h_{125}$ . Models in which also a coefficient  $c_{\text{uni}} > 1$  can be realized comprise, for instance, extensions of the SM by a real or complex  $\text{SU}(2)$  triplet Higgs field.

Under the assumption of the universal coupling coefficient  $c_{\text{uni}}$  and the presence of an invisible decay mode  $h_{125} \rightarrow \text{inv}$ , we can perform a  $\chi^2$ -fit to the measurements of the properties of  $h_{125}$  in dependence of the two free parameters  $c_{\text{uni}}$  and  $\text{BR}_{\text{inv}}$  with the help of `HiggsSignals`. By doing so, we obtain the two-dimensional  $\chi^2$ -distribution that is shown in Fig. 2. In this plot the color grading indicates the value of  $\Delta\chi^2$  in the parameter plane  $\{c_{\text{uni}}, \text{BR}_{\text{inv}}\}$ , and the solid and dashed lines indicate the 95% and the 68% CL limits, respectively. Also indicated with an orange star is the 95% CL upper limit  $\text{BR}_{\text{inv}} < 11\%$  which was obtained assuming a VBF production cross sections of  $h_{125}$  according to the SM prediction [33]. As such, the direct limit can in principle only be applied

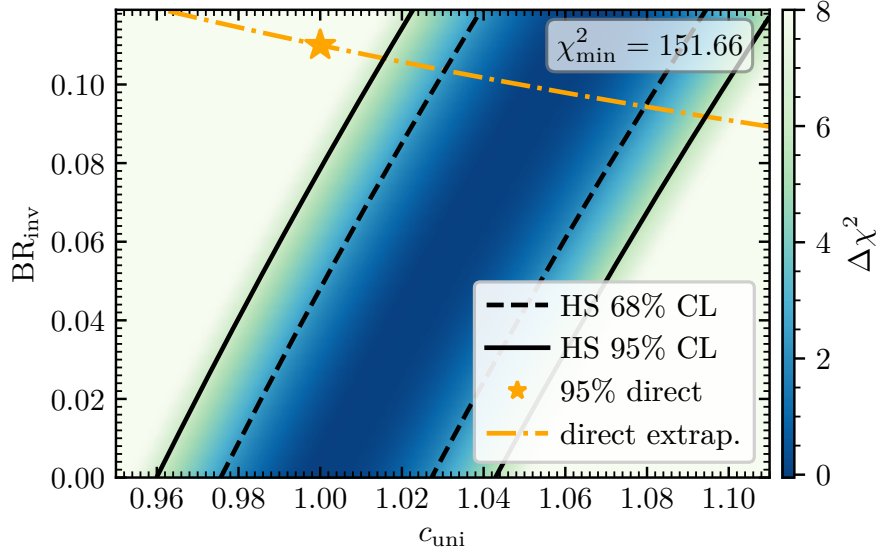


Figure 2: Result of the global fit to the Higgs signal-rate measurements assuming a Higgs boson  $h_{125}$  that has an invisible decay mode and whose couplings to the SM particles are modified w.r.t. the SM predictions by a universal coupling coefficient  $c_{\text{uni}}$ . The color coding indicates the value of  $\Delta\chi^2$  resulting from the `HiggsSignals` analysis. The black solid and dashed lines indicate the allowed regions at the 95% and the 68% confidence level, respectively. The orange star indicates the currently strongest upper limit on  $\text{BR}_{\text{inv}}$ , resulting from direct searches for  $h_{125} \rightarrow \text{inv}$  obtained according to the assumption that  $h_{125}$  is produced as predicted in the SM, i.e.  $c_{\text{uni}} = 1$  [33]. The orange dashed line indicates an approximate extrapolation of this direct limit for the case  $c_{\text{uni}} \neq 1$  (see text for details).

for  $c_{\text{uni}} = 1$ , in which case the production cross sections of the state at 125 GeV considered here agree with the SM predictions. However, for  $c_{\text{uni}} \neq 1$  the direct limit on  $\text{BR}_{\text{inv}}$  can still be applied in an approximate form. Taking into account that the VBF production cross section is given by  $\sigma_{\text{VBF}} = c_{\text{uni}}^2 \times \sigma_{\text{VBF}}^{\text{SM}}$  at leading order, with  $\sigma_{\text{VBF}}^{\text{SM}}$  being the SM cross section, the number of signal events would be enhanced or reduced by the factor  $c_{\text{uni}}^2$  depending on whether  $c_{\text{uni}}$  is larger or smaller than one, respectively. Under the assumption that the kinematical shape of the signal events is not modified substantially, which can be expected to be the case for small deviations of  $c_{\text{uni}}$  from unity, one can therefore apply the upper limit  $\text{BR}_{\text{inv}} < 11\%/c_{\text{uni}}^2$  from direct searches for  $h_{125} \rightarrow \text{inv}$  in order to account for the modification of the production cross section  $\sigma_{\text{VBF}}$  if  $c_{\text{uni}} \neq 1$ . We will call this limit an extrapolation of the direct limit on  $\text{BR}_{\text{inv}}$ , and this extrapolated limit is shown as the orange dotted-dashed line in Fig. 2.

One can see in Fig. 2 that there is a flat direction with  $\Delta\chi^2 \simeq 0$  in the  $\{c_{\text{uni}}, \text{BR}_{\text{inv}}\}$  plane. Along this flat direction, values of  $c_{\text{uni}} > 1$  give rise to an enhancement of the cross sections for the production of  $h_{125}$ , but at the same time values of  $\text{BR}_{\text{inv}} > 0$  suppress the decay modes of  $h_{125}$  decaying into SM particles (see also Ref. [44]). As a result, for each value of  $c_{\text{uni}} > 1$  there is a value of  $\text{BR}_{\text{inv}} > 0$  for which production cross sections times branching ratios remain equal to the SM predictions. Accordingly, we find that in the range  $c_{\text{uni}} \gtrsim 1.015$  the direct upper limit on  $\text{BR}_{\text{inv}}$  (orange lines) is stronger than the indirect limit on  $\text{BR}_{\text{inv}}$  resulting from the fit to the signal-rate measurements of  $h_{125}$ . For  $c_{\text{uni}} \gtrsim 1.085$  the values of  $\text{BR}_{\text{inv}}$  that are required in order to cancel the enhancement of the production cross sections of  $h_{125}$  are larger than the direct limit, such that the

combination of the indirect constraints from signal-rate measurements and the direct constraint on  $\text{BR}_{\text{inv}}$  is able to exclude this part of the parameter plane entirely.

In contrast to the case with  $c_{\text{uni}} > 1$ , in models in which the couplings of  $h_{125}$  are suppressed compared to the SM, i.e.  $c_{\text{uni}} < 1$ , one can observe that the indirect limit on  $\text{BR}_{\text{inv}}$  from the fit to the signal-rate measurements (black solid line) is always substantially stronger than the direct limit from searches for  $h_{125} \rightarrow \text{inv}$  (orange dotted-dashed line). In this region of the parameter plane, both the values of  $c_{\text{uni}} < 1$  and  $\text{BR}_{\text{inv}} > 0$  give rise to a suppression of the signal rates of  $h_{125}$ . This is why we observe that, the smaller the value of  $c_{\text{uni}}$ , the smaller is the indirect upper limit on  $\text{BR}_{\text{inv}}$  resulting from the signal-rate measurements of  $h_{125}$ . Finally we note that, according to the discussion of Sec. 2.1, also for  $c_{\text{uni}} = 1$  the indirect limit is stronger than the direct limit, as indicated with the orange star.

An approximate estimate of the allowed parameter space, corresponding to the region delimited by the two black lines in Fig. 2, is given at 95% CL by the condition

$$0.520 \text{BR}_{\text{inv}} + 0.960 < c_{\text{uni}} < 0.565 \text{BR}_{\text{inv}} + 1.043. \quad (2.8)$$

The fact that for  $c_{\text{uni}} < 1$  the indirect constraints provide the strongest constraints on  $\text{BR}_{\text{inv}}$ , whereas the direct limits are (in the considered scenario) essentially irrelevant, is important for phenomenological studies in models with extended Higgs sectors featuring a gauge-singlet scalar. Then the deviations of the universal coupling modifier  $c_{\text{uni}}$  to unity is generated via the mixing of the SM-like Higgs boson with the singlet scalar, and the coupling coefficient can be written as  $c_{\text{uni}} = \cos \theta \simeq 1 - \theta^2/2$  for small  $\theta$ , where  $\theta$  is the mixing angle. In such case, the constraints from Eq. (2.8) translate in very good approximation into

$$\text{BR}_{\text{inv}} < 0.078 \left( 1 - \left( \frac{\theta}{0.285} \right)^2 \right), \quad (2.9)$$

which implies that in the limit  $\text{BR}_{\text{inv}} \rightarrow 0$  values  $\theta < 0.285$  are excluded and reciprocally if  $\theta \rightarrow 0$ ,  $\text{BR}_{\text{inv}}$  is constrained to be  $\text{BR}_{\text{inv}} < 0.078$ , which is stronger than all current direct bounds listed in Tab. 1.<sup>11</sup> We will discuss the parameter constraints resulting from the analysis of this section in two concrete BSM theories, a hidden-sector composed of a fermionic DM candidate as well as a singlet scalar in Sec. 3.2, and a construction featuring (pseudo) Nambu-Goldstone bosons in Sec. 3.3.

### 2.3 $h_{125}$ with non-universally modified couplings and a non-zero $\text{BR}_{\text{inv}}$

In the previous section we investigated the case in which the couplings of the Higgs boson  $h_{125}$  are modified via a universal coupling coefficient  $c_{\text{uni}}$ . Although this procedure captures the modifications that arise in many BSM constructions featuring additional scalars, there is also a wide range of models in which the modifications to the couplings of  $h_{125}$  compared to the SM prediction cannot be captured in terms of a single coefficient. Since it is not feasible to use independent coupling modifiers for each of the couplings of  $h_{125}$ , we have to make assumptions on the total number of coupling modifiers that we include, and on how the couplings of  $h_{125}$  depend on these modifiers.

---

<sup>11</sup>If the invisible decay of  $h_{125}$  is absent, and modifications of the properties of  $h_{125}$  arise only by means of a universal coupling modification, we find in a one-dimensional parameter estimation 95% CL limits of  $c_{\text{uni}} > 0.968$ , or equivalently  $\theta < 0.253$ .

As already discussed in Sec. 2, for the case of non-universal coupling modifiers we will consider the four independent coefficients  $c_V$ ,  $c_u$ ,  $c_d$  and  $c_\ell$  defined in 2.3, and for the loop-induced couplings to gluons and photons we assume that no additional BSM loop-contributions play a role. Thus, including  $\text{BR}_{\text{inv}}$  as an additional free parameter, `HiggsSignals` can be used to determine  $\Delta\chi^2$  as a function of up to five independent parameters (see also Tab. 2 for a summary of the combinations of coupling modifiers for each case considered in this work). In order to be able to present the results in a clearer fashion, we will restrict our analysis in this section to parameter scans with only two independent coupling modifiers. The corresponding parameter space can be understood as a subspace of the more complicated coupling configurations allowed by the effective Lagrangian shown in 2.3, requiring further relations amongst the four individual coupling modifiers  $c_V$ ,  $c_u$ ,  $c_d$  and  $c_\ell$ . This approach allows us to show the allowed regions of the two varied parameters in two-dimensional plots, and we can investigate how these regions change with increasing values of  $\text{BR}_{\text{inv}}$ .

As a first example, we show constraints in a benchmark model commonly utilized by the CMS and the ATLAS collaborations (see, for instance, Ref. [3, 4, 59–61]), in which it is assumed that the couplings of  $h_{125}$  to fermions are modified by a common factor  $c_f = c_u = c_d = c_\ell$ , and, in addition, the coupling to the massive vector bosons is allowed to vary, i.e.  $c_V \neq 1$ . Such coupling modifications can be present in various different UV-complete BSM theories. For example, the presence of a gauge-singlet scalar that mixes with  $h_{125}$  gives rise to  $c_V = c_f < 1$ , as discussed in Sec. 2.2. Other examples comprise the 2HDM with Yukawa structure of type I and extensions thereof, where  $c_V \leq 1$ , and where  $c_f$  can be both smaller and larger than 1. Also extensions of the SM containing  $\text{SU}(2)$  triplet scalar fields that mix with the SM Higgs field can give rise to coupling modifications in terms of  $c_V$  and  $c_f$  as discussed above, where in contrast to 2HDMs also  $c_V > 1$  is possible (at tree level). All these models can be extended by a hidden sector in order to feature one or more valid DM particles, and where the Higgs sector can act as the portal between the hidden and the SM sector (see, for instance, Refs. [62–65]). Thus, if the decay of  $h_{125}$  into states of the hidden sector is kinematically allowed, it is interesting to analyze how the experimental limits on the coupling modifiers are modified for different values of the invisible branching ratio of  $h_{125}$ .

In Fig. 3 we show the values of  $\Delta\chi^2$  as a function of  $c_V$  and  $c_f$  for different choices of  $\text{BR}_{\text{inv}}$ . The upper left plot is obtained assuming that there is no invisible decay mode of  $h_{125}$ , and the other plots are obtained by increasing  $\text{BR}_{\text{inv}}$  in steps of 2% up to  $\text{BR}_{\text{inv}} = 10\%$  (lower right plot), covering the allowed range of  $\text{BR}_{\text{inv}}$  according to the direct limits. The solid and the dashed contours indicate the 95% and 68% CL exclusion limits based on the `HiggsSignals`  $\chi^2$ -fit to the cross-section measurements of  $h_{125}$ . One can see that with increasing value of  $\text{BR}_{\text{inv}}$  the allowed regions of the coupling modifiers move to larger values. This observation is in line with the discussion in Sec. 2.2, where we demonstrated that the suppression of the decay modes into SM particles due to the presence of the invisible decay mode can be compensated by an enhancement of the production cross sections as a result of coupling modifiers larger than one (see also Fig. 2). In contrast to the location of the allowed regions, the shape and the size of the allowed regions are practically unchanged in all plots. Furthermore, also the values of  $\Delta\chi^2$  featured by the best-fit points for the different values of  $\text{BR}_{\text{inv}}$  are effectively the same. Based on the results shown in Fig. 3, one can conclude that for BSM scenarios in which the restriction  $c_V \leq 1$  applies, the presence of the invisible decay mode gives rise to a decrease of the allowed ranges of both  $c_V$  and  $c_f$ . On the other hand, for models like the Higgs-triplet extension in which one can find values of  $c_V > 1$ , one can see that the presence of

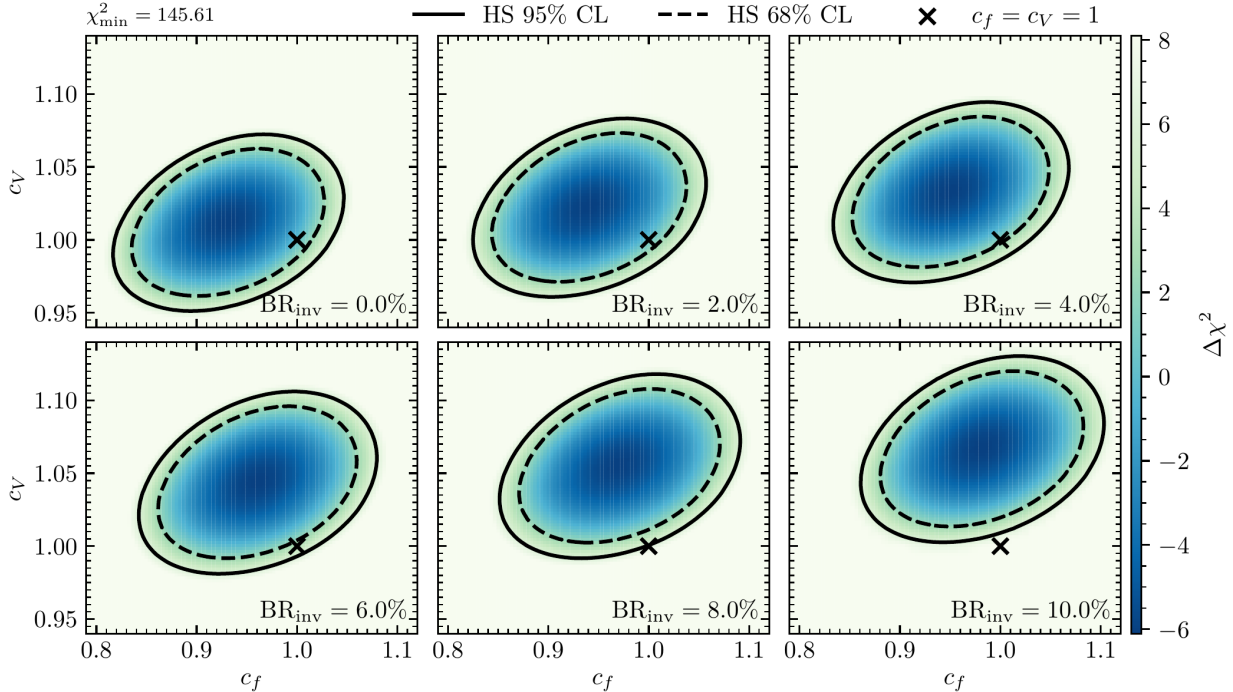


Figure 3: Result of the global fit to the Higgs-boson signal-rate measurements in the plane  $\{c_f, c_V\}$  for different values of  $\text{BR}_{\text{inv}}$ . The color coding indicates the value of  $\Delta\chi^2$  resulting from the `HiggsSignals` analysis. The black solid and dashed lines indicate the allowed regions at the 95% and the 68% confidence level, respectively. The black crosses indicate the point at which the couplings of  $h_{125}$  are identical to the SM predictions, i.e.  $c_f = c_V = 1$ .

an invisible decay mode of  $h_{125}$  with sizable branching ratios can open up parameter space regions that would be excluded if such a novel decay mode is not present. It should be noted also that the best-fit points do not lie at the point at which the couplings of  $h_{125}$  are identical to the SM predictions (black crosses) even if the decay mode  $h_{125} \rightarrow \text{inv}$  is absent. Instead, for  $\text{BR}_{\text{inv}} = 0\%$  the parameter points with the smallest values of  $\chi^2$  are found for  $c_V > 1$  and  $c_f < 1$ , featuring values of  $\Delta\chi^2 \approx -6$ .<sup>12</sup> Hence, if one would define the exclusion regions based on  $\Delta\chi^2 = \chi^2 - \chi^2_{\text{min}}$ , instead of  $\Delta\chi^2 = \chi^2 - \chi^2_{\text{SM}}$  as applied throughout this paper, one would obtain even stronger exclusion limits in the  $\{c_f, c_V\}$  plane (see also the related discussion in Sec. 2). The location of the best-fit points as a function of  $\text{BR}_{\text{inv}}$  moves to larger values of both coupling modifiers investigated here for increasing values of  $\text{BR}_{\text{inv}}$ .

A second BSM scenario that we consider is the case in which the coupling of  $h_{125}$  to gauge bosons is not modified compared to the SM predictions ( $c_V = 1$ ), in contrast to all the other scenarios discussed above, but in which the couplings to the fermions can deviate from the SM ( $c_u, c_d, c_\ell \neq 1$ ).

<sup>12</sup>The values of  $\Delta\chi^2 < 0$  are driven here by the following measurements, where for simplicity we only quote inclusive signal strength measurements here, and we remind the reader that  $\mu = 1$  according to the SM predictions: (i)  $\mu(\text{ttH}, H \rightarrow b\bar{b}) = 0.35^{+0.36}_{-0.34}$  reported by ATLAS [55], where it should be taken into account that the measurement uncertainty is dominated by systematic uncertainties regarding the background estimation, (ii)  $\mu(\text{ggH}, H \rightarrow \tau^+\tau^-) = 0.59^{+0.28}_{-0.32}$  and  $\mu(\text{VBF}, H \rightarrow \tau^+\tau^-) = 1.39^{+0.56}_{-0.47}$  reported by CMS [66], (iii)  $\mu(\text{ttH}) = 0.58^{+0.36}_{-0.33}$  reported by ATLAS [54], where the signal extraction is affected by the fact that the  $\text{ttW}$  background was found to be larger than the SM prediction.

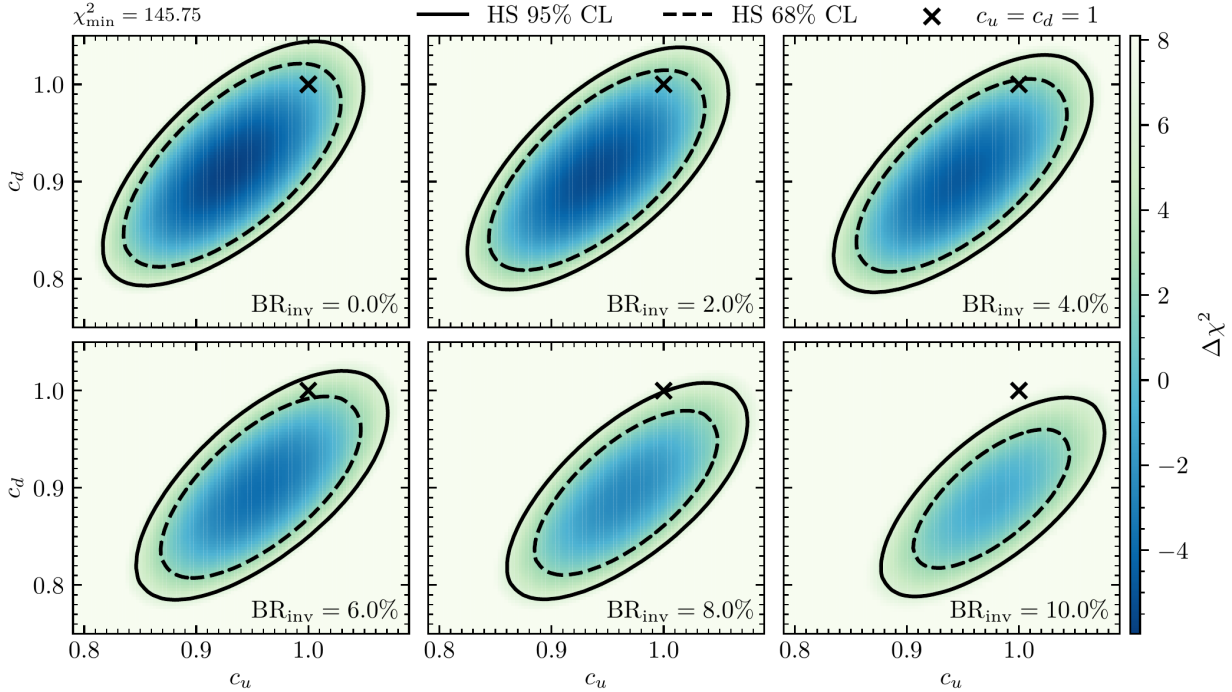


Figure 4: As Fig. 3, but in the plane  $\{c_u, c_d\}$  and assuming that  $c_\ell = c_d$  and  $c_V = 1$ .

We furthermore impose the condition  $c_\ell = c_d$  in order to stick to a parameter scan with two free parameters for a given value of  $\text{BR}_{\text{inv}}$ . UV-complete models in which coupling modifications of this form arise comprise generically extensions of the SM containing a second  $\text{SU}(2)$  doublet scalar field in which the so-called Yukawa structure of type II (see Sec. 3.4 for details) is imposed, which is also the Yukawa structure that arises in supersymmetric extensions of the SM (see e.g. Ref. [67]). We show the  $\chi^2$ -distribution in the  $(c_u, c_d)$  for different values of  $\text{BR}_{\text{inv}}$  as they were obtained with the help of `HiggsSignals` in Fig. 4, where the color coding and the definitions of the CL exclusion limits is as in Fig. 3. One can observe that increasing values of  $\text{BR}_{\text{inv}}$  shifts the allowed parameter regions to larger values of  $c_u$  and smaller values of  $c_d = c_\ell$ . The reason for the preference of larger values of  $c_u$  if  $\text{BR}_{\text{inv}} > 0$  lies in the fact that the enhancement of the coupling of  $h_{125}$  to top quarks gives rise to an enhancement of the gluon-fusion production cross section that partially compensates the suppression of the branching ratios for the ordinary decay modes of  $h_{125}$ . However, the VBF production mode, for instance, is unchanged since  $c_V = 1$ , such that the minimal values of  $\chi^2$  that are found for each value of  $\text{BR}_{\text{inv}}$  considered increase with  $\text{BR}_{\text{inv}}$ , in contrast to the results depicted in Fig. 3. The trend towards lower values of  $c_d$  with increasing values of  $\text{BR}_{\text{inv}}$  has its origin in the fact that a suppression of the coupling of  $h_{125}$  to bottom quarks suppresses the total width of  $h_{125}$ . As a consequence, sizable values of the decay width  $\Gamma_{\text{inv}}$  (see Eq. (2.1)) can be in agreement with the signal-rate measurements of  $h_{125}$ , because the measured branching ratios of the ordinary decays of  $h_{125}$  remain closer to the SM predictions. However, since  $c_V = 1$  and  $c_\ell = c_d$  in this scenario, the suppression of the couplings of  $h_{125}$  to tau leptons if  $c_d < 1$ , and the unchanged partial decay with for the decay modes  $h_{125} \rightarrow W^+W^-$  and  $ZZ$  still result in significant modifications of the branching ratios of  $h_{125}$  compared to the SM predictions, such that overall the fit result becomes worse with increasing values of  $\text{BR}_{\text{inv}}$ . As a result, even though for all possible values of  $\text{BR}_{\text{inv}}$  one can find



ranges of  $c_u$  and  $c_d$  that describe the experimental data regarding  $h_{125}$  as accurate as the SM, the size of the allowed regions of the coupling modifiers decreases and the fit result deteriorates with increasing value of  $\text{BR}_{\text{inv}}$ .

The two examples discussed above demonstrate that the presence of sizable values of  $\text{BR}_{\text{inv}}$  can improve or worsen the fit result to the Higgs-boson measurements, depending on which ranges of the coupling modifiers are considered, and depending on whether additional relations between the different modifiers are imposed. Since in both cases viable parameter ranges of the coupling modifiers survived even for values of  $\text{BR}_{\text{inv}} \simeq 10\%$ , it becomes apparent that both the direct and the indirect constraints on  $\text{BR}_{\text{inv}}$  have to be considered in order to be in agreement with the measurements regarding  $h_{125}$ . In Sec. 3.4 we will analyze the impact of the values of  $\text{BR}_{\text{inv}}$  on the allowed parameter regions in UV-complete models in which the couplings of the state at 125 GeV can be captured by the full set of coupling modifiers considered in our analysis, as defined in Eq. (2.3). Therein, as an illustrative example of popular BSM theories for which our results are relevant, we will focus on models containing, in addition to the hidden sector as the origin of the invisible decay mode of  $h_{125}$ , a second Higgs doublet.

### 3 Application to hidden sector models

In this section we will apply the indirect constraints on  $\text{BR}_{\text{inv}}$  obtained previously to concrete BSM scenarios featuring a hidden sector. We will start by considering Higgs-portal dark-matter models in Sec. 3.1 in which no coupling modifications of  $h_{125}$  are present, i.e.  $c_i = 1$ . As demonstrated in Sec. 2.1, in this case the indirect constraints on  $\text{BR}_{\text{inv}}$  are stronger than the direct constraints, such that the latter do not have to be considered. Afterwards we will discuss in Secs. 3.2–3.4 models featuring a hidden sector and an extended Higgs sector, in which the couplings of  $h_{125}$  to ordinary matter deviate from the SM predictions. Following the discussions in Sec. 2.2 and Sec. 2.3, here depending on the values of the coupling modifiers  $c_i$  predicted in each model, both the indirect or the direct constraints on  $\text{BR}_{\text{inv}}$  can be stronger, such that both constraints will have to be considered and their complementarity can be studied.

#### 3.1 The Higgs portal dark matter model

One of the simplest approaches to accommodate a valid DM candidate in a BSM scenario consists of the so-called Higgs portal scenario. Here it is assumed that the discovered Higgs boson  $h_{125}$  is the only portal to the dark sector, such that no direct (gauge) interactions with the SM fermions and the gauge bosons exist. We will consider here three possible kind of DM candidates coupled to the Higgs boson via  $\mathcal{L} = \mathcal{L}_{\text{SM}} + \mathcal{L}_{\text{DM}}$  where  $\mathcal{L}_{\text{SM}}$  is the SM Lagrangian and  $\mathcal{L}_{\text{DM}} = \mathcal{L}_S$  for real scalar DM ( $\equiv S$ ),  $\mathcal{L}_{\text{DM}} = \mathcal{L}_\chi$  for Dirac fermion DM ( $\equiv \chi$ ) and  $\mathcal{L}_{\text{DM}} = \mathcal{L}_V$  for real vector DM ( $\equiv V^\mu$ ) with

$$\mathcal{L}_S = -\frac{1}{4}\lambda_S|H|^2S^2, \quad \mathcal{L}_\chi = -\frac{1}{4}\frac{\lambda_\chi}{\Lambda}|H|^2\bar{\chi}\chi, \quad \mathcal{L}_V = -\frac{1}{4}\lambda_V|H|^2V^\mu V_\mu, \quad (3.1)$$

where  $\lambda_{S,\chi,V}$  and  $\Lambda$  are respectively dimensionless and dimension-one couplings. We parameterize the SM Higgs doublet in unitary gauge  $H = (0, v + h)^T/\sqrt{2}$  with  $v \simeq 246$  GeV and  $h = h_{125}$  is the SM Higgs boson. In addition, in each of the three cases we consider bare mass terms for our DM candidates. We will denote the physical scalar, fermion and vector dark-matter masses

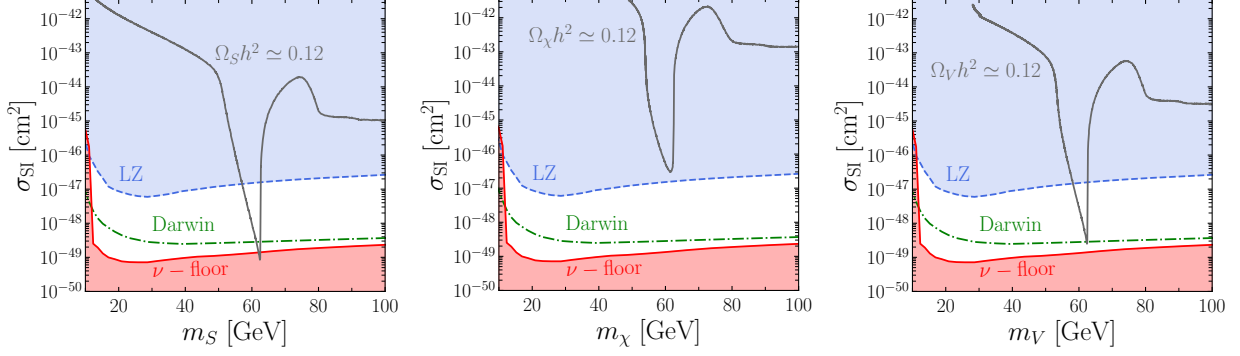


Figure 5:  $\sigma_{\text{SI}}$  as a function of the DM mass for the Higgs-portal parameter space in which the relic abundance as observed by Planck is reproduced (dark grey), for scalar DM (left), Dirac fermion DM (center) and vector DM (right). Constraints from LZ, projection for Darwin and the neutrino floor are represented in blue (dashed), green (dotted-dashed) and red (solid) respectively.

after electroweak symmetry breaking by  $m_{S,\chi,V}$ , respectively. The partial widths of the Higgs-boson decays into a pair of DM particles are given by <sup>13</sup>

$$\begin{aligned}
 \Gamma_{h \rightarrow SS} &= \frac{\lambda_S^2 v^2}{128\pi m_h} \left(1 - \frac{4m_S^2}{m_h^2}\right)^{1/2}, \\
 \Gamma_{h \rightarrow \bar{\chi}\chi} &= \frac{\lambda_\chi^2 v^2 m_h}{128\pi \Lambda^2} \left(1 - \frac{4m_\chi^2}{m_h^2}\right)^{3/2}, \\
 \Gamma_{h \rightarrow VV} &= \frac{\lambda_V^2 v^2 m_h^3}{512\pi m_V^4} \left(1 - 4\frac{m_V^2}{m_h^2} + 12\frac{m_V^4}{m_h^4}\right) \left(1 - \frac{4m_V^2}{m_h^2}\right)^{1/2}.
 \end{aligned} \tag{3.2}$$

Higgs-portal models are strongly constrained by the null-results of direct-detection experiments. Currently, the most stringent experimental constraints on the DM-nucleon spin-independent scattering cross section  $\sigma_{\text{SI}}$  were reported by the Xenon1T [14], PandaX-4T [15] and the LUX-ZEPLIN (LZ) experiments [16], whose most recent results exclude  $\sigma_{\text{SI}} \gtrsim 10^{-47} \text{ cm}^2$  for a 50 GeV DM mass and up to  $\sigma_{\text{SI}} \gtrsim 10^{-45} \text{ cm}^2$  for 10 TeV DM mass. The sensitivity of the upcoming Darwin experiment [70] should improve the current bounds from LZ by more than an order of magnitude, and will almost reach the so-called neutrino floor [71]. The direct detection cross section with a nucleon  $N$ , mediated by the Higgs boson, can be expressed for the three scenarios considered here as

$$\sigma_{\text{SI}}^S = \frac{\lambda_S^2 \mu_{SN}^2 m_N^2}{16\pi m_S^2 m_h^4} f_N^2, \quad \sigma_{\text{SI}}^\chi = \frac{\lambda_\chi^2 \mu_{\chi N}^2 m_N^2}{16\pi \Lambda^2 m_h^4} f_N^2, \quad \sigma_{\text{SI}}^V = \frac{\lambda_V^2 \mu_{VN}^2 m_N^2}{16\pi m_V^2 m_h^4} f_N^2, \tag{3.3}$$

with  $\mu_{AB} = m_A m_B / (m_A + m_B)$ .<sup>14</sup> The nucleon form factor  $f_N \sim 0.3$  is defined as  $f_N \equiv f_{T_u}^{(N)} + f_{T_d}^{(N)} + f_{T_s}^{(N)} + (6/27)f_{T_G}^{(N)}$  where  $f_{Tq}^{(N)} \equiv \langle N | m_q \bar{q}q | N \rangle / m_N$  is the contribution from a quark  $q$  to the nucleon mass and  $f_{T_G}^{(N)} \equiv 1 - \sum_q f_{Tq}^{(N)}$  is the gluon contribution.<sup>15</sup>

<sup>13</sup>The expression for the scalar DM is in agreement with Ref. [20] and Ref. [68]. The expression for the vector DM is in agreement with Ref. [69].

<sup>14</sup>The expression for scalar DM is in agreement with Ref. [20, 23, 68], and the one for vector DM is in agreement with Refs. [23, 69]

<sup>15</sup>Numerical values for these form factor can be found in Ref. [72].

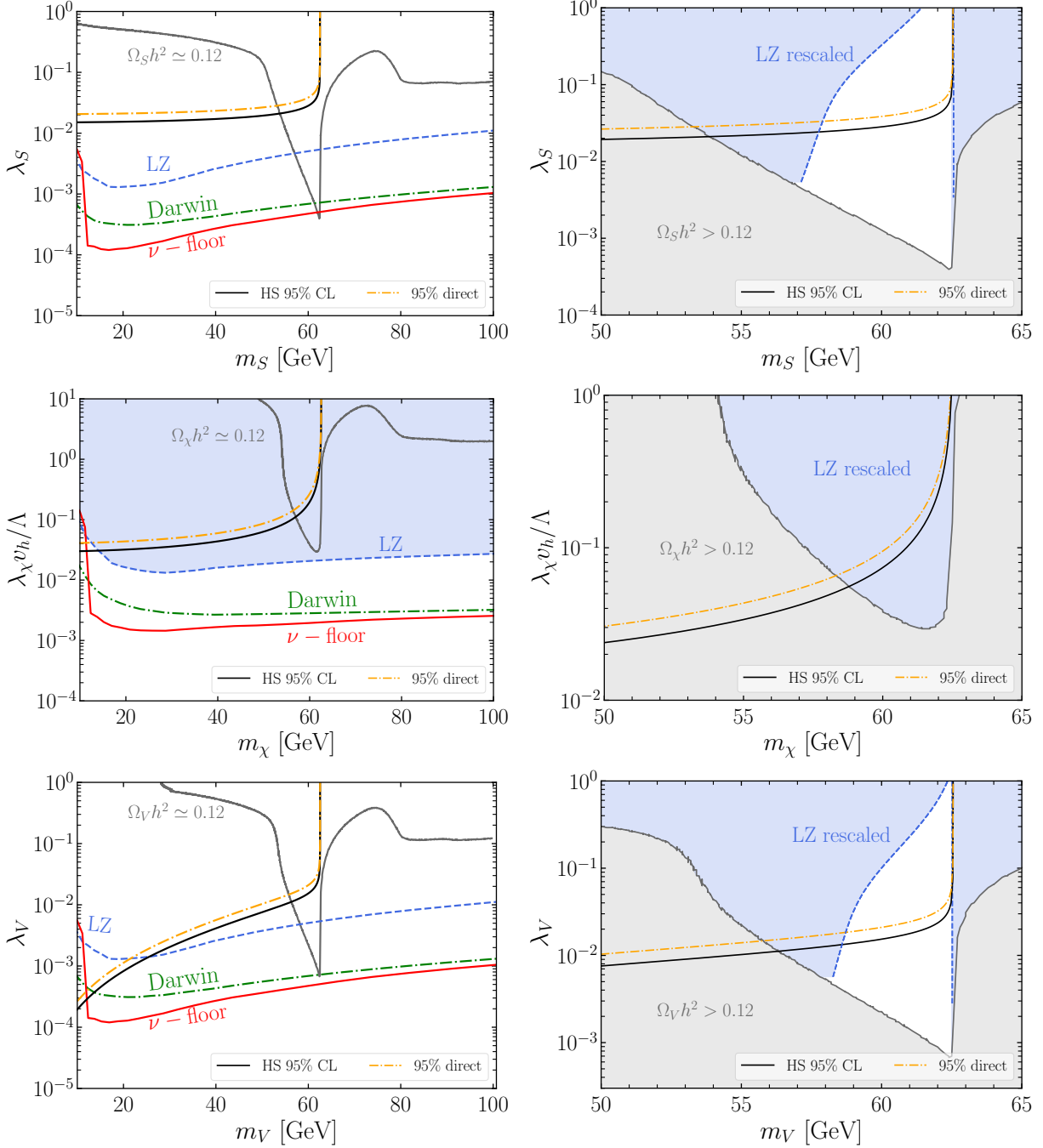


Figure 6: Higgs-portal parameter plane of dimensionless couplings and the DM mass for scalar DM  $S$  (first row), Dirac fermion DM  $\chi$  (second row) and vector DM  $V$  (third row). The dark-grey lines indicates the parameter space reproducing the relic abundance as observed by Planck. Constraints from LZ, projection for Darwin and the neutrino floor are represented in dashed blue, dotted-dashed green and solid red respectively. In the plots on the right, the LZ constraint is rescaled according to the predicted DM abundance via Eq. (3.4), and the light-grey areas represent regions where the DM relic abundance exceeds the Planck value. The solid black and dotted-dashed orange lines represent respectively our constraints derived using `HiggsSignal` and constraints from direct searches for the invisible decay of  $h_{125}$ .

After implementing the models in `Feynrules` [73], we used `micrOMEGAs` [74, 75] to compute numerically both relic abundance and direct detection cross sections.<sup>16</sup> In Fig. 5 we represented with a dark gray line in the plane  $\{\sigma_{\text{SI}}, m_{S,\chi,V}\}$  the parameter points that satisfy the relic density as determined by the Planck collaboration [12] within a  $3\sigma$  interval around the best-fit value,  $\Omega_\chi h^2 \in [0.11933 - 3 \times 0.00091, 0.11933 + 3 \times 0.00091]$  for the three kind of dark matter candidates of the Higgs portal scenarios considered in this work. We also indicate the constraints from LZ in dashed blue, sensitivity prediction for Darwin in dotted-dashed green and the neutrino floor in solid red. From Fig. 5, one can see that the Higgs portal models considered in this section are essentially only allowed for bosonic dark matter candidates and for a very narrow region of DM masses close to the resonance  $m_\chi \simeq m_h/2 \simeq 62.5$  GeV, if one assumes that the dark matter abundance saturates the Planck best fit value. The fermionic dark matter candidate considered in this section is entirely excluded by the most recent results from the LZ collaboration.

We represented the relic density and direct detection constraints in the left panels of Fig. 6 in terms of a dimensionless coupling as a function of the DM mass. In addition, we represented constraints on Higgs physics from `HiggsSignal` and direct limits from ATLAS respectively in black and dotted-dashed orange line. For a given set of parameters, one can rescale the LZ constraints according to the predicted value for the relic abundance via

$$\sigma_{\text{SI}}^{\text{LZ}} = \sigma_{\text{SI}}^{\text{LZ}}|_{\Omega_{\text{DM}}h^2=0.11933} \left( \frac{0.11933}{\Omega_{\text{DM}}h^2} \right), \quad (3.4)$$

where  $\sigma_{\text{SI}}^{\text{LZ}}|_{\Omega_{\text{DM}}h^2=0.11933}$  is the LZ constraint assuming a DM abundance  $\Omega_{\text{DM}}h^2 = 0.11933$  and  $\Omega_{\text{DM}}h^2$  is the DM abundance predicted for a given set of parameters. The rescaled LZ constraint is represented on the plots in the right panels of Fig. 6 where the blue areas represent the excluded regions. One can see from this figure that such constraint weakens precisely around the peak value for bosonic DM candidates, as a smaller DM abundance  $\Omega_{\text{DM}}h^2 < 0.11933$  is generated in this region. However, the fermionic dark matter candidate is completely excluded, even if it constitutes just a fraction of the total dark matter.<sup>17</sup>

One can relax the condition of achieving the correct relic abundance via a single Higgs-portal parameter by assuming the presence of additional DM annihilation channels as typically expected in constructions featuring a more complex hidden sector. In this case, the correct relic abundance could be achieved for a smaller value of the Higgs-portal dimensionless coupling. As can be seen in the left panels of Fig. 6, constraints from Higgs physics would become the strongest, for fermion and vector DM, in the region of the parameter space corresponding to masses  $\lesssim m_h/2$ . In addition, if one assumes a multi-component dark matter setup, direct detection constraints would have to be rescaled according to the local density of the relevant dark matter component. The parameter space at small masses  $\lesssim m_h/2$  could open up and the constraints derived in this work would become the strongest.

<sup>16</sup>With `micrOMEGAs`, we obtained numerical results for the direct detection cross section within a 10% agreement with respect to our analytical expression of Eq. (3.3).

<sup>17</sup>Notice that in this work we considered a scalar operator  $\bar{\chi}\chi$  connected to the Higgs field. Our statement here depends on the choice of operators and could differ, for example, for a pseudoscalar operator  $\bar{\chi}\gamma_5\chi$ . It remains to be investigated whether one can evade the LZ constraints upon inclusion of the pseudoscalar operator, or whether the presence of new mediators between the hidden sector and the visible sector at or below the electroweak scale have to be introduced in order to predict a viable fermionic Higgs-portal DM scenario [76] (see also Sec. 3.2).

In such cases, for DM masses typically  $\lesssim m_h/2$ , our constraints derived using `HiggsSignal`, independent of the local dark matter density, could be stronger than both direct detection bounds and from an extrapolation of direct searches for a invisible decay of the Higgs boson.

### 3.2 Singlet portal dark matter

The simplest possibility to extend the Higgs portal DM scenario is to assume the presence of an additional real singlet scalar field  $\Phi$  that can act as a portal between the dark sector and the visible sector. This can be achieved by considering a discrete  $\mathbb{Z}_4$  symmetry acting on  $\Phi \rightarrow -\Phi$  [38] and by introducing components of a fermionic Dirac DM candidate  $\chi_{L,R}$  with opposite chiralities  $\chi \equiv \chi_L + \chi_R$  that couples to  $\Phi$  via

$$\mathcal{L} \supset -y_\chi \Phi \bar{\chi}_L \chi_R + \text{h.c.}, \quad (3.5)$$

where  $y_\chi$  is a Yukawa coupling.<sup>18</sup> The most general scalar potential respecting the  $\mathbb{Z}_4$  symmetry is given by

$$V = \mu_H^2 H^\dagger H + \frac{1}{2} \mu_\Phi^2 \Phi^2 + \lambda_H (H^\dagger H)^2 + \frac{1}{4} \lambda_\Phi \Phi^4 + \frac{1}{2} \lambda_{\Phi H} \Phi^2 H^\dagger H, \quad (3.6)$$

where  $\mu_{H,\Phi}$  and  $\lambda_{H,\Phi,\Phi H}$  are respectively dimension-one and dimensionless parameters.  $H$  is a  $SU(2)$  Higgs doublet, following the same notation as in the previous section. The quartic coupling  $\lambda_{\Phi H}$  in combination with the Yukawa interaction of Eq. (3.5) allow for the interactions between the DM candidate and the SM. The  $\mathbb{Z}_4$  symmetry is spontaneously broken down to a remaining  $\mathbb{Z}_2$  symmetry by the vacuum expectation value (vev) of the singlet field  $\langle \Phi \rangle = v_\phi$ . We parametrize the scalar field as  $\Phi = v_\phi + \phi$  where  $\phi$  denotes a real scalar degree of freedom. The singlet vev  $v_\phi$  generates a mass term  $m_\chi = y_\chi v_\phi$  for the DM fermion, whose stability is ensured by the remaining  $\mathbb{Z}_2$  symmetry. In the following, we will assume that no bare mass term for the DM fermion is present (or equivalently that it can be neglected), such that the physical mass of  $\chi$  is given by  $m_\chi$ . In order to obtain the physical mass eigenstates  $h_{1,2}$  an orthogonal field transformation can be performed, parameterized by an angle  $\theta$

$$\begin{pmatrix} h_1 \\ h_2 \end{pmatrix} = \begin{pmatrix} c_\theta & -s_\theta \\ s_\theta & c_\theta \end{pmatrix} \begin{pmatrix} h \\ \phi \end{pmatrix}, \quad (3.7)$$

with  $s_\theta \equiv \sin \theta$  and  $c_\theta \equiv \cos \theta$ . The expression for the mixing angle  $\theta$  in terms of the vevs and the quartic scalar couplings and details about the minimization of the scalar potential are given in App. A. In the following, the physical state  $h_1 \simeq h_{125}$  denotes the neutral scalar whose mass is identical to the discovered Higgs boson, i.e.  $m_{h_1} \simeq 125$  GeV, but with couplings modified by factors of  $c_{\text{uni}} = \cos \theta$  with respect to the SM prediction. In the following the mixing angle  $\theta$  is taken as free parameter in combination with the physical masses  $m_{h_1}$  and  $m_{h_2}$  and the vev of the singlet  $v_\phi$ . Taking into account that the Yukawa coupling  $y_\chi$  is fixed by the DM mass  $m_\chi = y_\chi v_\phi$  if  $v_\phi$  is used as free parameter, we are left with  $(m_{h_1}, m_{h_2}, m_\chi, v_\phi, \theta)$  as set of independent free parameters.

Both physical scalars mediate DM-nucleon scatterings whose corresponding cross section can be expressed as

$$\sigma_{\text{SI}} = \frac{\mu_{\chi N}^2}{\pi} \left[ \frac{m_N m_\chi}{v v_\phi} c_\theta s_\theta \left( \frac{1}{m_{h_2}^2} - \frac{1}{m_{h_1}^2} \right) \right]^2 f_N^2. \quad (3.8)$$

<sup>18</sup>Under the  $\mathbb{Z}_4$  symmetry, the two chirality components of  $\chi$  would transform as  $\chi_R \rightarrow i\chi_R$  and  $\chi_L \rightarrow -i\chi_L$ .

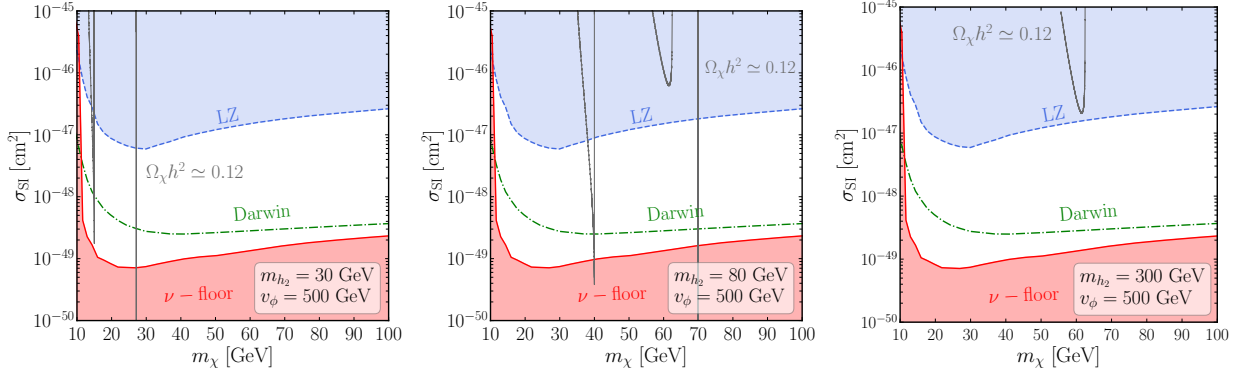


Figure 7: As in Fig. 5 for the singlet portal DM scenario for different values of the mass of the additional scalar  $m_{h_2}$  and the vev  $v_\phi$ .

where notations are identical to the ones used in Sec. 3.1. In Fig. 7 we represented the value of the direct detection cross section as a function of the dark matter mass for the parameter space allowing to reproduce the correct relic abundance for selected value of  $v_\phi$  and  $m_{h_2}$  as dark-grey lines.<sup>19</sup> In Fig. 7 the resonances correspond to DM annihilating via (quasi) on-shell mediators ( $h_1$  and  $h_2$ ) and therefore are peaked around  $m_\chi \simeq m_{h_1}/2 \simeq 62.5$  GeV and  $m_\chi \simeq m_{h_2}/2$ . The vertical lines at  $m_\chi \simeq 30$  GeV in the left plot and  $m_\chi \simeq 80$  GeV in the middle plot, respectively, have their origin in the channel  $\bar{\chi}\chi \rightarrow h_2 h_2$  opening, which is kinematically forbidden at zero temperature for  $m_\chi < m_{h_2}$  and exponentially suppressed at finite temperature but yet still efficient enough to yield the correct relic abundance. For this annihilation channel the DM abundance is set by the value of the Yukawa coupling between the fermionic DM and the singlet scalar, which also sets the DM mass resulting in  $\theta$ -independent generated relic abundance. Larger DM masses correspond to larger annihilation cross sections and a resulting dark matter under-abundance.

We also indicate in Fig. 7 the currently strongest upper limit on  $\sigma_{\text{SI}}$  from the LZ collaboration with the blue shaded region. One can see that the LZ constraints exclude most parts of the parameter space that predicts the experimentally determined DM relic abundance. In the scenario with  $m_{h_2} < m_{h_1}/2$  (left plot) and  $m_{h_1}/2 < m_{h_2} < m_{h_1}$  (middle plot) only DM masses of  $m_\chi \simeq m_{h_2}/2$  and  $m_\chi \lesssim m_{h_2}$  remain viable, whereas the scenario with  $m_{h_2} > m_{h_1}$  (right plot) is entirely ruled out in the low-mass regime investigated here. Thus, we will not discuss the latter scenario any further in the following.

In the singlet portal dark matter model the presence of a second scalar particle gives rise to additional experimental constraints that have to be applied. The Higgs boson  $h_1 \simeq h_{125}$  can decay invisibly into a dark matter pair, but  $h_1$  can also decay into pairs of light scalars  $h_2$  if  $m_{h_2} < m_{h_1}/2$ . Depending on whether the singlet-like state  $h_2$  decays predominantly into SM particles or into DM pairs, the decay mode  $h_1 \rightarrow h_2 h_2$  either gives rise to exotic visible decay modes of  $h_1$ , mainly resulting in  $b\bar{b}b\bar{b}$ ,  $b\bar{b}\tau^+\tau^-$  and  $b\bar{b}\mu^+\mu^-$  final states, or the decay mode  $h_1 \rightarrow h_2 h_2$  gives rise to an additional invisible decay mode of  $h_1$ . The decay rates for the decays of  $h_1$  into BSM states are given in App. A.2. Accordingly, the additional Higgs boson  $h_2$  can be searched for via the decays  $h_1 \rightarrow h_2 h_2$  if kinematically allowed in the final states mentioned above. In addition,  $h_2$  can be

<sup>19</sup>The DM-nucleon scattering cross sections obtained with the analytical expression shown in Eq. (3.8) are in agreement within 10% with the results obtained using the public code `micrOMEGAs` [74, 75].

directly searched for at  $pp$  colliders via its production in the ggH or VBF production modes and at lepton colliders via Higgsstrahlung production. Therefore, we here also include constraints from collider searches for additional Higgs bosons by using the public code `HiggsBounds` [47, 77–80], which are complementary to the constraints resulting from the signal-rate measurements of  $h_1$ .

We present in Fig. 8 the constraints from the Higgs-boson measurements using `HiggsSignal` and from searches for additional Higgs bosons using `HiggsBounds`. The top-panels show  $\Delta\chi^2$  obtained with `HiggsSignal`, and the corresponding upper bounds on the mixing angle as a function of the dark matter mass for selected value of  $v_\phi$  and  $m_{h_2}$  at the 68% and the 95% CL indicated by the black dashed and solid lines, respectively. We also indicate the region which is excluded by the observed 95% CL cross-section limits with regards to  $h_2$  with the red line, where the regions above the red lines are excluded (further details are given below). Finally, the orange dotted-dashed lines indicate the regions at which the predicted invisible branching ratio of the discovered Higgs boson at 125 GeV are equal to the upper limit obtained from direct searches for the invisible decay mode, i.e.  $\text{BR}_{\text{inv}} = 11\%$ . As mentioned above, here  $\text{BR}_{\text{inv}}$  is determined by adding the contributions from the decay modes  $h_1 \rightarrow \bar{\chi}\chi$  and  $h_1 \rightarrow h_2 h_2 \rightarrow \bar{\chi}\chi\bar{\chi}\chi$  if kinematically allowed. One can see that in both scenarios the indirect constraints on  $\text{BR}_{\text{inv}}$  from the cross-section measurements of  $h_{125}$  (black lines) are stronger than the direct limit on  $\text{BR}_{\text{inv}}$  for all DM masses considered.

The lower panels show the same exclusion lines superimposed to the parameter space allowed by the LZ bounds, and in which the correct relic abundance (dark grey) or a lower value (light grey) is achieved. As discussed in Sec. 3.1, the LZ constraints are rescaled according to Eq. (3.4). According to the previous discussion, the parameter space allowed by the LZ constraints corresponds to two different regimes: a narrow region around  $m_\chi \simeq m_{h_2}/2$  where DM annihilation is resonantly enhanced by  $s$ -channel diagrams and the region  $m_\chi \simeq m_{h_2}$  where  $\bar{\chi}\chi \rightarrow h_2 h_2$  DM annihilation processes are efficient enough in order to not overclose the universe. In the following, we discuss in more detail the two benchmark scenarios with  $m_{h_2} < m_{h_1}/2$  (left) and  $m_{h_1}/2 < m_{h_2} < m_{h_1}$  (right) that are depicted in Fig. 8.

**A second Higgs boson below 125/2 GeV:** In the scenario depicted in the left panels of Fig. Fig. 8, the decay of the SM-like Higgs boson  $h_1$  into a pair of scalars  $h_2$  is kinematically allowed, which mainly determines the exclusions obtained from the experimental data regarding  $h_1 \simeq h_{125}$ . For DM masses of  $2m_\chi > m_{h_2} = 30$  GeV, the scalar  $h_2$  decays to visible final state (mostly  $\bar{b}b$ ). If  $2m_\chi > m_{h_1} \simeq 125$  GeV the `HiggsSignals` constraint ( $\theta < 0.073$  at 95% CL) is then insensitive to the DM mass. For  $m_\chi \lesssim m_{h_2}/2$ , the invisible decay channel  $h_2 \rightarrow \bar{\chi}\chi$  becomes relevant, such that  $\text{BR}_{\text{inv}} > 0$  and one finds slightly stronger constraints on  $\theta$  from the cross-section measurements of  $h_{125} \simeq h_1$ . One can compare the indirect constraints from the cross-section measurements of  $h_{125}$ , indicated by the black line, to the exclusions from the direct constraint  $\text{BR}_{\text{inv}} < 11\%$  obtained from searches for the invisible decay of  $h_{125}$ , indicated by the orange line. The direct limit on  $\text{BR}_{\text{inv}}$  gives rise to two disconnected exclusion regions. The parameter space above the right parabola-shaped orange line is excluded because the decay mode  $h_1 \rightarrow \chi\bar{\chi}$  has a branching ratio larger than 11%. The second exclusion region is the parameter space that lies within the closed orange line at  $m_\chi < 15$  GeV, in which additionally the decay mode  $h_1 \rightarrow h_2 h_2 \rightarrow \chi\bar{\chi}\chi\bar{\chi}$  contributes to  $\text{BR}_{\text{inv}}$ . However, both exclusion regions resulting from the direct limit on  $\text{BR}_{\text{inv}}$  lie above the black line and are therefore already excluded based on the signal-rate measurements of  $h_{125}$ . Finally, the

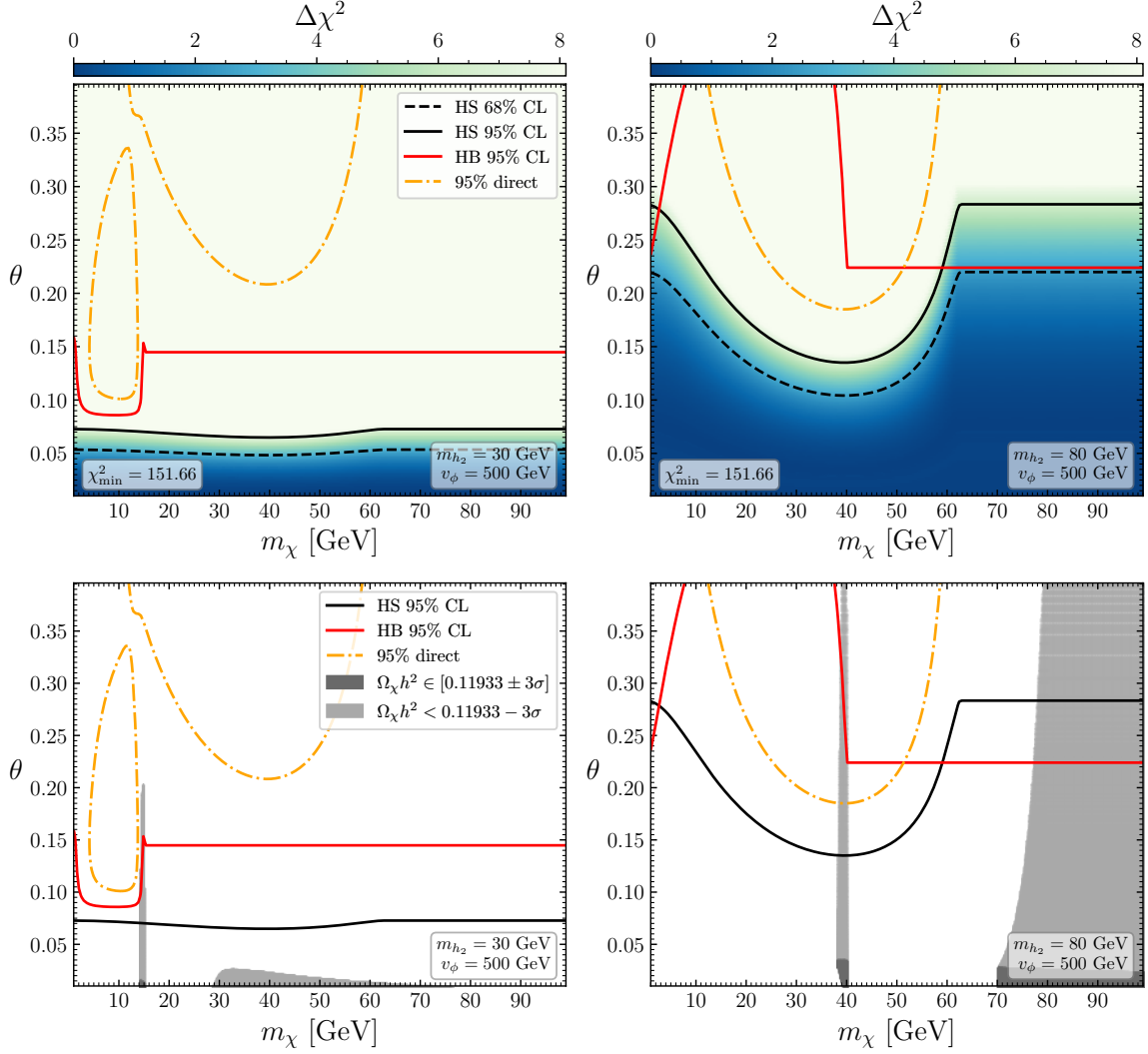


Figure 8: In the upper plots we show  $\Delta\chi^2$  in the  $\{m_\chi, \theta\}$  plane for two different choices of  $m_{h_2}$  and  $v_\phi$ . The resulting exclusion limits at 95% and 68% CL are shown with solid and dashed black lines, respectively, excluding the areas above the lines. The 95% CL exclusion region from searches for additional scalars is shown in red, excluding the areas above the lines. The parameter points for which  $\text{BR}_{\text{inv}}$  is equal to the upper limit from direct searches for the invisible decay of  $h_{125}$  are indicated with the orange lines. In the lower plots we additionally indicate the parameter space allowing to reproduce all (dark grey) or part of (light grey) the measured relic abundance.

exclusions as a consequence of the searches for additional Higgs bosons, indicated by the red line, have their origin in two different collider searches. For  $m_\chi > 15$  GeV we find an upper limit of  $\theta \lesssim 0.15$  due to constraints from searches for Higgs-boson decays into a pair of two lighter scalars in the  $b\bar{b}\mu^+\mu^-$  final state performed by the ATLAS collaboration at 13 TeV [81]. For  $m_\chi < 15$  GeV we find a substantially stronger limit of  $\theta \lesssim 0.10$  from searches for invisibly decaying scalars performed by the OPAL collaboration at the LEP collider at up to 209 GeV [82]. However, for all values of  $m_\chi$  considered the constraints from the searches for additional Higgs bosons are weaker than the constraints determined with HiggsSignals.



**A second Higgs boson below 125 GeV:** Whereas in the previous case the indirect constraints from the  $h_{125}$  measurements were dominantly determined by the presence of the decay mode  $h_2 \rightarrow h_1 h_1$ , in the benchmark scenario depicted in the right plot of Fig. 8 this decay is kinematically not possible. Thus, the constraints depend, on the one hand, on the presence of the mixing between  $h_1$  and  $h_2$ , and, on the other hand, also on the presence of the invisible decay  $h_1 \rightarrow \chi\bar{\chi}$  if  $2m_\chi < 125$  GeV. We find that the `HiggsSignal` constraints (black line) are weaker at large DM masses  $m_\chi > m_{h_1}/2$ , yielding an upper limit of  $\theta < 0.29$ . This limit is only set by modifications of the SM prediction of the Higgs-boson universal couplings and matches our results from Sec. 2.2 of Eq. (2.9). The invisible decay of the SM-like Higgs boson opens up for  $m_\chi < m_{h_1}/2$ , and the exclusion line from the `HiggsSignals` analysis drops below the one from `HiggsBounds` (red line) at DM masses below about 60 GeV. With regards to the direct limit on  $\text{BR}_{\text{inv}}$  (orange line), the island of an excluded region at  $m_\chi < 15$  GeV disappears in the right plot, since only the invisible decay  $h_1 \rightarrow \bar{\chi}\chi$  is kinematically allowed, whereas the decay  $h_1 \rightarrow h_2 h_2$  is not possible, leaving only the parabolic-shaped upper bound set by the invisible decay of the Higgs boson  $h_{125}$ . As before, the indirect constraints from the cross-section measurements of  $h_{125}$  are always stronger than the constraints from the direct limit on  $\text{BR}_{\text{inv}}$ . In contrast to the previous case, we find for  $m_{h_2} > m_{h_1}/2$  that the `HiggsBounds` analysis excluded parameter regions that otherwise would be allowed. In the right plot, with  $m_{h_2} = 80$  GeV, we find an upper limit of  $\theta \lesssim 0.225$  as a result of the cross section limits from searches for scalar particles produced via Higgsstrahlung production and decaying into pairs of bottom quarks performed at LEP [83].<sup>20</sup> The exclusion power of this search becomes much weaker for  $m_\chi < 40$  GeV, where the scalar  $h_2$  is able to decay into pairs of  $\chi$  and the branching ratio for the decay  $h_2 \rightarrow b\bar{b}$  is smaller.

In this section we have considered a discrete  $\mathbb{Z}_4$  symmetry as a specific example. However this construction could be extended by considering instead a global continuous  $U(1)$  symmetry, broken spontaneously. In this case the imaginary part of the complex scalar field responsible for the symmetry breaking would be a massless Goldstone boson. The analysis performed in this section would not be drastically affected by the presence of this new state but would need to be accounted for in the possible DM annihilation final states. Constraints from Higgs physics would have to be modified as the SM-like Higgs boson could decay into a pair of Goldstone bosons. This precise point is discussed in the following subsection.

### 3.3 (Pseudo) Nambu-Goldstone bosons

In this section we consider a model with an additional (approximate) global  $U(1)$  symmetry and a complex scalar field parameterized in the exponential form by  $\Phi = (v_\phi + \phi)e^{ia/v_\phi}/\sqrt{2}$ , singlet under the SM gauge group but charged under the new global  $U(1)$ . All SM fields are singlets under the additional  $U(1)$  symmetry. The scalar potential including all terms that respect this symmetry has the same form as the one of Eq. (3.6), and we adopt the same notation as in Sec. 3.2. Depending on the specificity of the model, the global symmetry could be spontaneously broken ( $v_\phi \neq 0$ ) or not ( $v_\phi = 0$ ). If the symmetry is spontaneously broken, a mixing by an angle  $\theta$  between the real part

<sup>20</sup>In addition, the `HiggsBounds` analysis provides constraints that are stronger than the ones from `HiggsSignals` at  $m_\chi \lesssim 3$  GeV, where however the dark-matter direct-detection constraints already rule out the relevant part of the parameter space. The most sensitive search as determined by `HiggsBounds` here is the search for invisibly decaying scalars at LEP performed by the L3 collaboration [84].

of the complex field and the Higgs field is generated, while the state  $a$  is a Nambu-Goldstone Boson (NGB) or Pseudo Nambu-Goldstone Boson (PNGB) depending on whether the broken symmetry was exact or approximate before spontaneous symmetry breaking. In the latter case, we assume that any explicit symmetry breaking term is small compared to the electroweak scale such that the mass of the (P)NGB can be set to zero in the following analysis. Using the exponential parametrization, the field  $a$  disappears from the scalar potential and the only coupling between the Higgs boson at 125 GeV and the (P)NGB is generated via mixing from the kinetic terms of the scalar  $\Phi$  after spontaneous symmetry breaking [85, 86],

$$\mathcal{L} \supset |\partial_\mu \Phi|^2 = \frac{1}{2} \left( \partial_\mu \phi \partial^\mu \phi + \partial_\mu a \partial^\mu a \left( \frac{\phi^2}{v_\phi^2} + 2 \frac{\phi}{v_\phi} + 1 \right) \right), \quad (3.9)$$

before performing a rotation to the mass eigenstate basis. We obtain canonically normalized kinetic terms for the massless pseudoscalar field  $a$  in addition to higher dimensional operators involving derivative couplings. One can perform a rotation to the physical CP-even neutral scalar mass eigenstate basis  $\{h_1, h_2\}$  by considering the transformation described in the previous section (see Eq. (3.7)). By selecting only terms relevant for the decay of the SM-like Higgs boson into pairs of (P)NGBs, one obtains

$$\mathcal{L} \supset \frac{1}{2} \partial_\mu a \partial^\mu a \left( 1 - 2 \frac{s_\theta h_1}{v_\phi} \right) \supset -\partial_\mu a \partial^\mu a \frac{s_\theta h_1}{v_\phi}. \quad (3.10)$$

This parametrization makes obvious that the decay into pairs of (P)NGBs of the SM-like Higgs state is triggered by the mixing angle  $\theta$ . The coupling term of Eq. (3.10) generates a partial decay width

$$\Gamma_{h_1 \rightarrow aa} = \frac{s_\theta^2}{32\pi} \frac{m_{h_1}^3}{v_\phi^2}. \quad (3.11)$$

One can recover this result by choosing the linear parametrization  $\Phi = (v_\phi + \phi + ia)/\sqrt{2}$  and by expressing the scalar potential of Eq. (3.6) in terms of the mass eigenstates, as performed in Ref. [64].

As the couplings between the SM field content and the Higgs boson  $h_1 \simeq h_{125}$  are modified by a universal factor  $c_{\text{uni}} = \cos\theta$ , we can derive constraints in the plane  $\{\cos\theta, (v_\phi/m_{h_1})\}$ , where we divide the vev  $v_\phi$  by  $m_{h_1} = 125$  GeV in order to have a dimensionless quantity. We depict in Fig. 9 with the color coding the  $\Delta\chi^2$ -values from `HiggsSignals` in this plane. In addition, we show with the black dashed and solid lines the resulting exclusion limits at the 68% and 95% CL, respectively, and we also show exclusion lines based on perturbative unitarity constraints on the dimensionless coupling of the scalar potential for a selection of masses  $m_{h_2} = v_\phi/2, v_\phi, 2v_\phi$  (explicit expressions for these constraints can be found, for instance, in Ref. [87]).<sup>21</sup> In agreement with the discussions of Sec. 2.2, we find that the indirect constraints from the cross-section measurements of  $h_{125}$  are considerably stronger than constraints from the experimental limit on  $\text{BR}_{\text{inv}}$  from direct searches for the invisible decay of  $h_{125}$ , where the latter are indicated with the orange dashed-dotted line in Fig. 9. For instance, for  $v_\phi/m_{h_1} = 10$  we find that the mixing angle is constrained to be  $\cos\theta > 0.99$  or equivalently  $\theta < 0.14$  at 95% CL based on the values of  $\Delta\chi^2$ , whereas the bounds from direct searches for the decay  $h_{125} \rightarrow \text{inv}$  allow for values as small as  $\cos\theta > 0.98$  or equivalently  $\theta < 0.20$ . As can be seen in Eq. (3.11), in the limit where the ratio  $v_\phi/m_{h_1}$  becomes large, the partial width

<sup>21</sup>The  $m_{h_2}$  dependence of these limits enters via the relations shown in Eqs. (A.5)–(A.6).

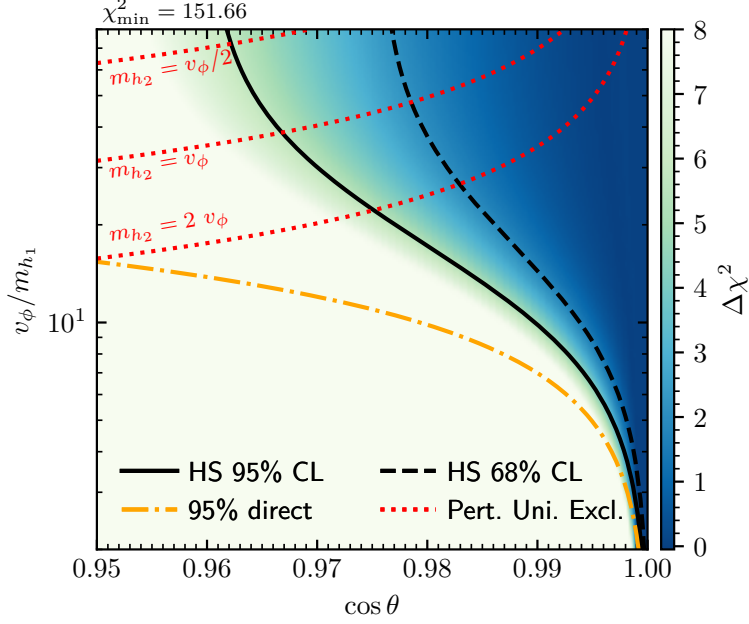


Figure 9:  $\Delta\chi^2$ , indicated by the colour coding, in the  $\{\cos\theta, v_\phi/m_{h_1}\}$  plane for the (Pseudo) Nambu-Goldstone boson scenario. The resulting exclusion limits at 95% and 68% CL are shown respectively with solid and dashed black lines, excluding the areas below the lines. Areas below the orange dashed line are excluded based on the experimental limit on  $\text{BR}_{\text{inv}}$  from direct searches for  $h_{125} \rightarrow \text{inv}$ . The areas above the dotted red lines are excluded by constraints from perturbative unitarity assuming  $m_{h_2} = v_\phi/2, v_\phi, 2v_\phi$  (see discussion in Sec. 3.3 for details).

for the invisible decay of  $h_1 \simeq h_{125}$  becomes negligible. Accordingly, in this limit the bound on the mixing angle saturates at a constant value of  $\cos\theta > 0.959$  which matches our results derived in Sec. 2.2 of Eq. (2.8) in the limit  $\text{BR}_{\text{inv}} \rightarrow 0$ . The limits on  $\cos\theta$  can be even stronger when one combines the limits from the cross-section measurements of  $h_{125}$  with the perturbative unitarity constraints. For instance, assuming that  $m_{h_2} = v_\phi$  imposes  $\cos\theta > 0.966$ , corresponding to  $\theta < 0.26$ .

It is tempting to demand independent limits on  $\text{BR}_{\text{inv}}$  and  $\theta$  in a phenomenological analysis in order to account in an approximate form for the experimental constraints, on the one hand, from the invisible decay mode of  $h_{125}$  and, on the other hand, from the mixing between  $h_{125}$  and the additional scalar state. In many studies this amounts to applying the direct limit on  $\text{BR}_{\text{inv}}$  (orange line) and a constant lower limit on the coupling modifier  $c_{\text{uni}} = \cos\theta (> 0.959)$ , where the value in the brackets is the limit we found to be valid in the limit  $\text{BR}_{\text{inv}} \rightarrow 0$  according to the discussion above. The results depicted in Fig. 9 illustrate that this approach would allow substantial parts of the parameter space that are actually excluded by the cross-section measurements of  $h_{125}$  (black line). This demonstrates that in order to fully exploit the experimental data with regards to the discovered Higgs boson in models with light hidden sectors it is vital to take into account *simultaneously* the presence of a non-zero  $\text{BR}_{\text{inv}}$  and the modifications of the couplings of  $h_{125}$  to SM particles, as was done in our global  $\chi^2$ -analysis using `HiggsSignals`.

The results derived in this section go beyond the global symmetry case and can also be applied to the case of a local  $U(1)$  gauge symmetry to some extent. In the regime where the mass of the new light vector state  $m_{Z'} = g_{Z'} q_\phi v_\phi \ll m_{h_{125}}$ , with  $g_{Z'}$  being the extra  $U(1)$  gauge coupling and  $q_\phi$  the

Model	$u_R$	$d_R$	$\ell_R$
Type I	$\Phi_2$	$\Phi_2$	$\Phi_2$
Type II	$\Phi_2$	$\Phi_1$	$\Phi_1$
Type III (lepton-specific)	$\Phi_2$	$\Phi_2$	$\Phi_1$
Type IV (flipped)	$\Phi_2$	$\Phi_1$	$\Phi_2$

Table 3: Summary of which of the two Higgs doublet fields  $\Phi_{1,2}$  is coupled to up-type fermions ( $u_R$ ), down-type fermions ( $d_R$ ) and charged leptons ( $\ell_R$ ) in the four Yukawa types of the 2HDM.

charge of the complex scalar breaking this symmetry, by virtue of the Goldstone boson equivalence theorem the decay rate  $\Gamma_{h_{125} \rightarrow aa}$  into a pair of Goldstone bosons  $a$  is identical to the rate  $\Gamma_{h_{125} \rightarrow Z'Z'}$  into a pair of massive gauge fields  $Z'$  in the small mass limit. Therefore, our constraints also apply to this case, provided that the produced  $Z'$  is sufficiently weakly coupled in order to escape the detector without interacting.

### 3.4 Two Higgs doublet models

One of the most prominent example where observables related to the Higgs boson depart from their SM predicted values are models containing two Higgs doublet fields  $\Phi_1$  and  $\Phi_2$ , called 2 Higgs doublet models (2HDM) [88, 89] (see also Ref. [90] for a review). In the CP-conserving 2HDM, the physical Higgs spectrum consists of two CP-even states  $h$  and  $H$ , where  $h$  in the following plays the role of  $h_{125}$ , a CP-odd state  $A$ , and a pair of charged Higgs bosons  $H^\pm$ . In the decoupling limit of the 2HDM, in which the BSM particle states have masses considerably larger than the electroweak scale, the couplings of the state  $h = h_{125}$  to the fermions and gauge bosons are determined by only two parameters: the ratio of the vacuum expectation values of the neutral CP-even components of the Higgs doublets  $v_1$  and  $v_2$  written in terms of the parameter

$$\tan \beta \equiv \frac{v_2}{v_1}, \text{ where } v = \sqrt{v_1^2 + v_2^2} \simeq 246 \text{ GeV}, \quad (3.12)$$

and the rotation angle  $\alpha$  that determines the mixing of the two CP-even states  $h$  and  $H$ . In the so-called alignment limit, defined by the condition  $\cos(\alpha - \beta) = 0$ , the couplings of  $h$  to the SM particles are identical to the predictions of the SM.

In order to eliminate sources of flavour-changing neutral currents at the classical level, one can introduce a softly broken  $\mathbb{Z}_2$  symmetry, under which one of the Higgs doublets changes sign, whereas the second Higgs doublet transforms trivially, and the  $\mathbb{Z}_2$  charges of the fermions depend on the so-called Yukawa type that is assumed. In total, there are four different possibilities to assign the fermion charges. Depending on the fermion charge, either  $\Phi_1$  or  $\Phi_2$  can be coupled to the corresponding fermion. In Tab. 3 we explicit which Higgs doublet field is coupled to which kind of fermion in each of the four types of the 2HDM considered in this work. The resulting structure of the coupling modifiers that is realized in each Yukawa type is given in Tab. 2. The explicit dependence of the modifiers  $c_{V,u,d,\ell}$  on the parameters  $\alpha$  and  $\beta$  can be found, for instance, in Ref. [90].

In the following we perform a  $\chi^2$ -scan in the plane  $\{\cos(\alpha - \beta), \tan \beta\}$  for the four types of the 2HDM in the decoupling limit, and we analyze how the allowed regions of parameter space are modified by the existence of an invisible decay mode of  $h$ . The resulting constraints in terms of exclusion

regions can be applied to a variety of 2HDMs that are extended by a hidden sector. Such models comprise, for instance, scalar gauge-singlet extensions of the 2HDM such as the N2HDM [91], the S2HDM [65, 92] or the 2HDM+a [93]. Here it should be taken into account that for a concrete model realization of a particular configuration of 2HDM-like coupling modifications also other experimental and theoretical constraints would have to be considered. We refrain from doing such a model-specific analysis here, as we want to focus on the constraints that arise from the properties of  $h_{125}$  under the presence of an additional invisible decay mode.

**Type I** We show in the upper plots of Fig. 10 the  $\chi^2$ -distribution in the  $\{\cos(\alpha - \beta), \tan \beta\}$  plane for the Yukawa type I for different values of  $\text{BR}_{\text{inv}}$  (varied in steps of 2%). The black dashed and solid lines indicate the excluded regions of the model parameters at the 68% and the 95% CL, respectively. One can see that, as expected, the best agreement with the experimental data regarding  $h_{125}$  is found at or about the alignment limit  $\cos(\alpha - \beta) = 0$ , in which the state  $h$  resembles a SM Higgs boson. By comparing the plots for different values of  $\text{BR}_{\text{inv}}$  it becomes apparent that the values of  $\Delta\chi^2$  increase with increasing values of  $\text{BR}_{\text{inv}}$  in the whole parameter plane. Consequently, in the Yukawa type I the presence of an invisible decay mode of  $h_{125}$  deteriorates the fit result to the experimental Higgs-boson data independently of the values of the coupling modifiers. For a value of  $\text{BR}_{\text{inv}} = 6\%$  only a small region with  $\tan \beta \lesssim 5$  and  $\cos(\alpha - \beta) \simeq 0$  remains allowed at the  $1\sigma$  level, whereas for  $\text{BR}_{\text{inv}} = 8\%$  even the alignment limit is almost excluded at the 95% CL. The type I Yukawa structure is excluded at more than 95% CL for  $\text{BR}_{\text{inv}} = 10\%$ , such that the experimental limits from direct searches for  $h_{125} \rightarrow \text{inv}$  (currently at the level of  $\text{BR}_{\text{inv}} < 11\%$  or larger) do not provide additional constraints. The observations made here are in agreement with the results depicted in Fig. 3 for the scan in the benchmark model featuring the coupling modifiers  $c_V$  and  $c_f = c_u = c_d = c_\ell$ , which is also the pattern of coupling modifications that is realized in the type I, where here the additional restriction  $c_V \leq 1$  applies. Accordingly, we also observe here values of  $\Delta\chi^2$  substantially smaller than zero. The origin of these values was discussed already in Sec. 2.3.

**Type II** The corresponding results for the Yukawa type II are depicted in the bottom panels of Fig. 10. Regarding the fit result in the vicinity of the alignment limit of the Yukawa type II, one can observe that with increasing value of  $\text{BR}_{\text{inv}}$  the parameter region that is in agreement with the measurements of  $h_{125}$  moves towards values of  $\cos(\alpha - \beta) > 0$ . This is related to the fact that one finds  $|c_b| < 1$  and  $|c_V| \simeq |c_u| \simeq 1$  for  $\cos(\alpha - \beta) > 0$ , such that the additional contribution  $\Gamma_{\text{inv}}$  to the total decay width of  $h_{125}$  is compensated by a reduced partial decay width  $\Gamma_{b\bar{b}}$ , while at the same time the ggH and the VBF production cross sections of  $h_{125}$  are not significantly modified compared to the SM predictions. On the other hand, for  $\cos(\alpha - \beta) < 0$  one finds  $|c_d| > 1$ , such that the branching ratio of the decay  $h_{125} \rightarrow \gamma\gamma$  is suppressed by both the non-zero value of  $\Gamma_{\text{inv}}$  and the enhancement of  $\Gamma_{b\bar{b}}$ , and consequently the fit result deteriorates in this case with increasing values of  $\text{BR}_{\text{inv}}$ .

In the type II, in addition to the alignment limit, there is a tight branch in the parameter plane with values of  $\cos(\alpha - \beta) > 0.08$  and  $\tan \beta \gtrsim 7$  that predicts a state  $h$  that can be in agreement with the experimental measurements and hence features small values of  $\Delta\chi^2$ . This branch is a 2HDM realization of the so-called *wrong-sign Yukawa coupling regime*, in which the absolute values of the coupling modifiers are approximately equal to one, i.e.  $|c_{V,u,d,\ell}| \simeq 1$ , but in which the couplings

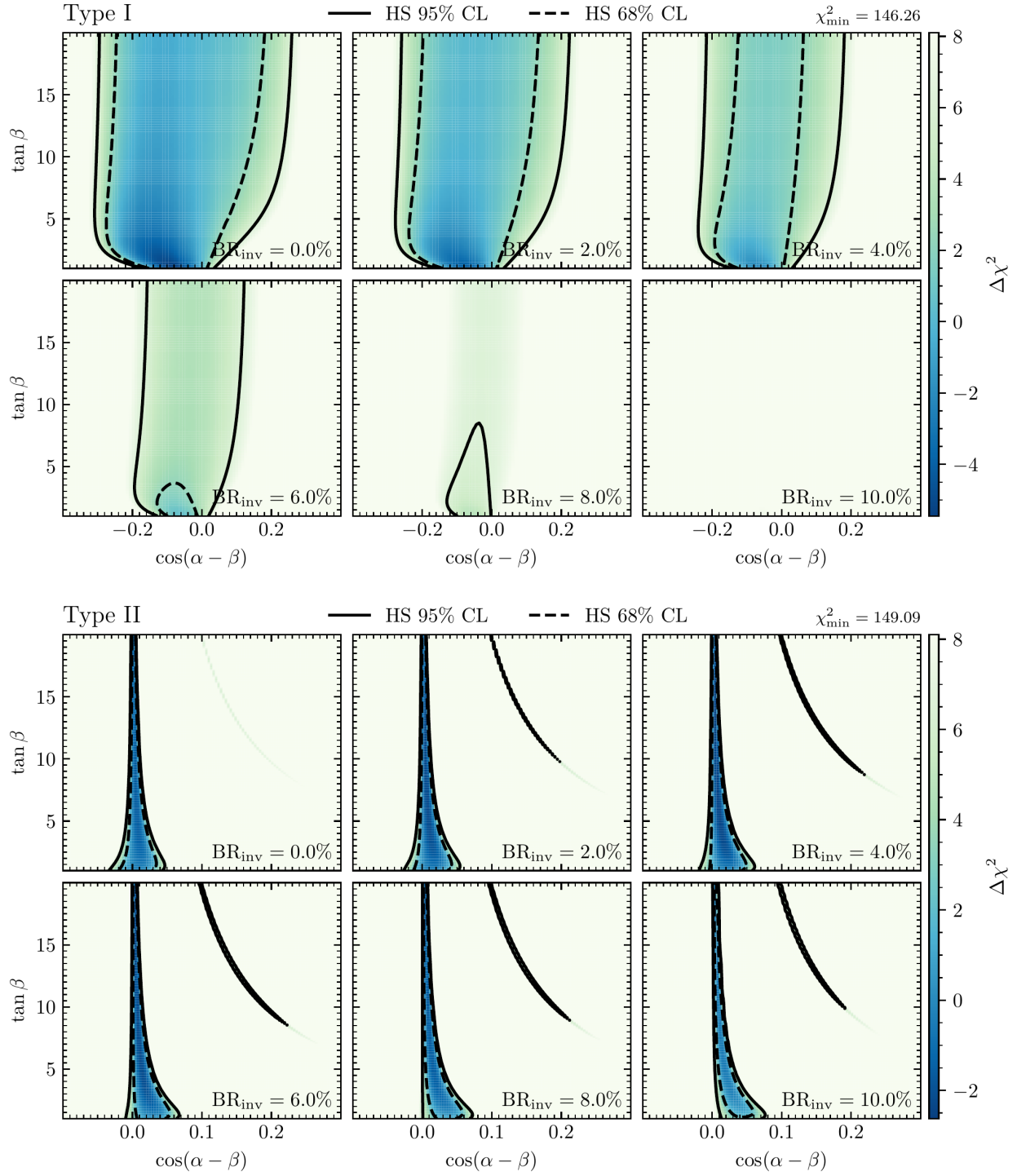


Figure 10:  $\Delta\chi^2$ -distribution in the  $\{\cos(\alpha - \beta), \tan\beta\}$  plane for different values of  $BR_{inv}$  in the type I (top) and the type II (bottom). The dashed black and the solid black lines indicate the exclusion limits at the 68% and the 95% confidence level, respectively.

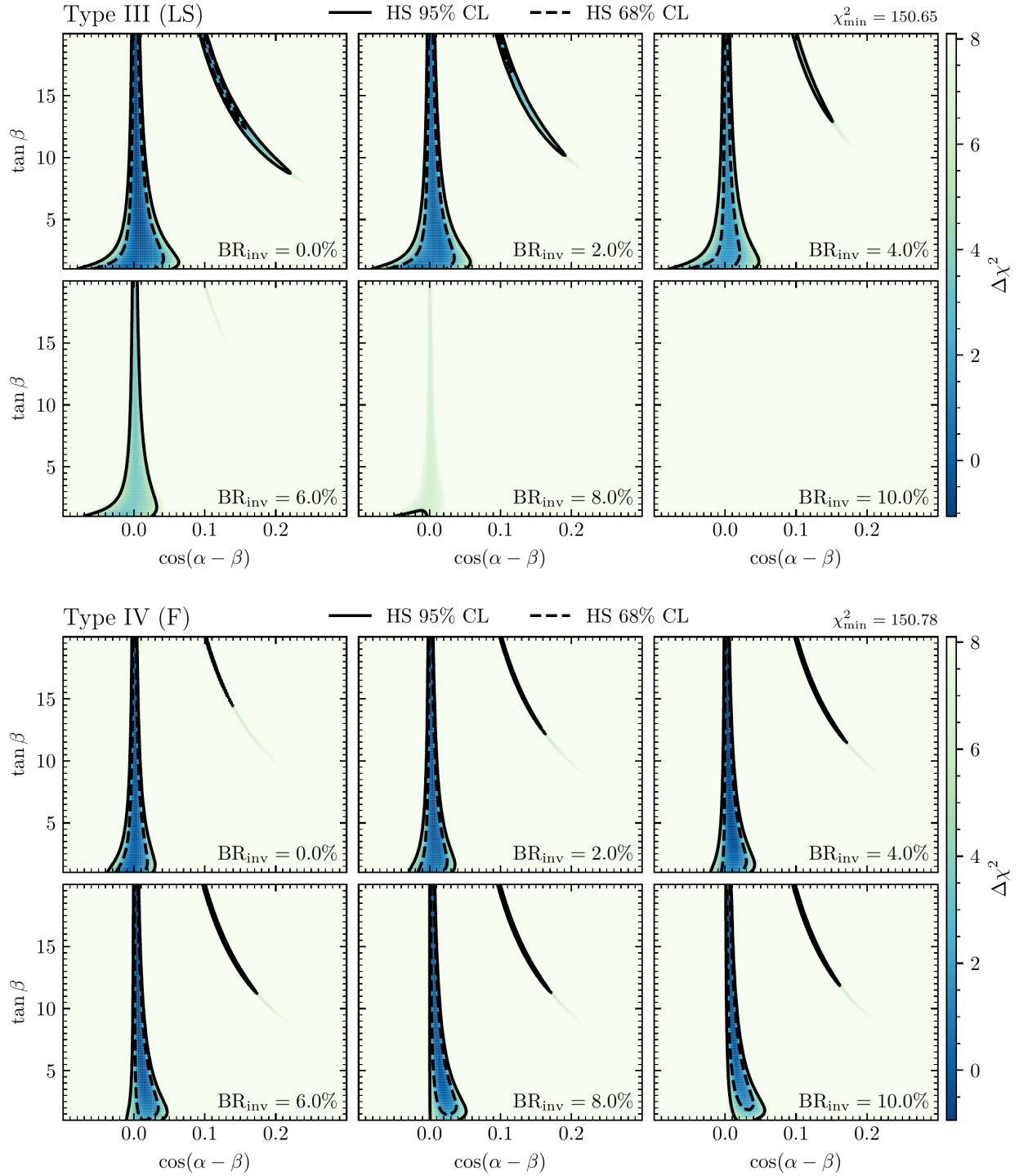


Figure 11: Same as in Fig. 10, but for the type III (top) and the type IV (bottom).

to down-type quarks have the opposite sign as compared to the couplings to gauge bosons and up-type quarks [42, 94] (see also Ref. [95] for a discussion of this limit in the 2HDM in light of recent LHC measurements). In the absence of a decay mode  $h_{125} \rightarrow \text{inv}$  the wrong-sign Yukawa coupling regime is in tension with the signal-rate measurements of  $h_{125}$ , as can be seen in the upper left plot. This tension is mainly driven by the enhancement of the gluon-fusion production cross section of  $h_{125}$  compared to the SM prediction as a result of the modified interference effects between the contributions from the top-quark loop and the bottom-quark loop [95]. We find here that the agreement with the experimental data can be improved significantly in the wrong-sign Yukawa coupling regime if a sizable value of  $\text{BR}_{\text{inv}}$  is present. Even for values as large as  $\text{BR}_{\text{inv}} = 10\%$  we find parameter points in this limit that fit the signal-rate measurements of  $h_{125}$  just as well as the SM, whereas the same parameter points would be excluded at a CL substantially larger than  $2\sigma$  for  $\text{BR}_{\text{inv}} = 0$ . Here, the additional partial decay with  $\Gamma_{\text{inv}}$  leads to a suppression of the ordinary decay modes of  $h_{125}$  which compensates the enhancements of the gluon-fusion production cross sections. The relative sizes of the signal rates of  $h_{125}$  can then remain close to the SM predictions because the type II Yukawa structure allows for the individual modification of both  $c_u$  and  $c_d$ , such that one can find  $|c_u| \simeq |c_V| \simeq 1$  and  $|c_d| < 1$  (compare also to Fig. 4 and the related discussion).

As a consequence of the fact that we find both in the vicinity of the alignment limit and in the wrong-sign Yukawa coupling regime parameter points that are in agreement with the indirect constraints from the signal-rate measurements of  $h_{125}$  even for values of  $\text{BR}_{\text{inv}} = 10\%$ , whereas the same parameter points would be excluded in the absence of the invisible decay mode, it becomes clear that in the Yukawa type II the upper limits on  $\text{BR}_{\text{inv}}$  from the direct searches for  $h_{125} \rightarrow \text{inv}$  are (and will be) relevant and have to be taken into account. Finally, we emphasize that in order to find a valid parameter point in the allowed parameter regions for  $\text{BR}_{\text{inv}} > 0$  in a concrete BSM theory also other constraints, for instance, from LHC searches for the BSM Higgs bosons  $H$ ,  $A$  and  $H^\pm$  would have to be checked against. We will leave such a model-specific analysis for future investigations.

**Type III** The results for the type III (lepton-specific) Yukawa structure are depicted in the top panels of Fig. 11. The couplings of  $h_{125}$  to vector bosons and to up- and down-type quarks in type III are identical to the ones in type I. Thus, the predictions for the production cross sections of  $h_{125}$  are very similar to type I. Accordingly, we find for type III that the agreement with the indirect constraints becomes worse with increasing value of  $\text{BR}_{\text{inv}}$ , similarly to what we observed for type I (see Fig. 10). This is also true for the wrong-sign Yukawa coupling regime, which cannot be realized in type I, whereas, as can be seen in the top row of plots in Fig. 11, in type III the wrong-sign Yukawa coupling regime is still allowed with regards to the constraints from the signal-rate measurements of  $h_{125}$ . However, in contrast to what we observed in type II, in type III the fit-result in the wrong-sign Yukawa coupling regime becomes worse with increasing value of  $\text{BR}_{\text{inv}}$ , and it is effectively absent for values of  $\text{BR}_{\text{inv}} > 6\%$ . We find that for  $\text{BR}_{\text{inv}} = 8\%$  only a small region around the alignment limit remains allowed if exclusion limits at the 95% CL are applied. For  $\text{BR}_{\text{inv}} = 10\%$  the whole parameter plane is excluded in type III. Hence, in this case the upper limits on  $\text{BR}_{\text{inv}}$  resulting from the direct searches for  $h_{125} \rightarrow \text{inv}$  do not provide additional constraints, and one should instead apply the indirect constraints resulting from the signal-rate measurements of  $h_{125}$ .



**Type IV** The results for the Yukawa type IV (flipped) are depicted in the bottom panels of Fig. 11. In this type, the coupling modifiers  $c_V$ ,  $c_u$  and  $c_d$  are identical to the ones of the Yukawa type II. As a result, the cross-section predictions are also (practically) identical, and also the main branching ratios of  $h_{125}$  remain effectively unchanged compared to type II, with the exception of the decays of  $h_{125}$  into pairs of charged leptons. Accordingly, we find that the allowed region in the  $\{\cos(\alpha - \beta), \tan \beta\}$  plane resemble the allowed regions that we found for type II (see Fig. 10). Both in the vicinity of the alignment limit, but also in the wrong-sign Yukawa coupling regime, we find allowed regions that accommodate the experimental data regarding  $h_{125}$  within the  $1\sigma$  level. Hence, as in type II, the direct limit  $\text{BR}_{\text{inv}} < 11\%$  from the searches for the  $h_{125} \rightarrow \text{inv}$  decay mode have to be taken into account in type IV, since they exclude parameter space points with larger values of  $\text{BR}_{\text{inv}}$  that otherwise would be allowed.

## 4 Summary and conclusions

We explored the possibility of connecting a hidden sector to the discovered Higgs boson at 125 GeV. We parameterized deviations of the Higgs-boson couplings to SM states by introducing coupling modifiers  $c_i$  for  $i = V, u, d, \ell$ , and by introducing a possible invisible branching ratio  $\text{BR}_{\text{inv}}$  as a free parameter. We performed  $\chi^2$ -analyses taking into account a large set of cross-section and signal-rate measurements of the discovered Higgs boson by using the public code `HiggsSignals`, and we identified the ranges of the coupling modifiers that are allowed or excluded at 68% and 95% confidence level depending on the value of  $\text{BR}_{\text{inv}}$ . We furthermore derived constraints on generic constructions of modifications of the properties of  $h_{125}$  compared to the SM, by making general assumptions about the structure of the couplings, in order for the corresponding constraints to be applicable to a large category of models. Finally, we derived constraints on the model parameters for a variety of more specific BSM constructions featuring hidden sectors such as Higgs-portal dark matter models, scenarios featuring Nambu-Goldstone bosons and extended Higgs sector in the context of the 2HDM.

The first general conclusion of this paper is that currently in a wide class of models the LHC measurements of the signal rates of conventional visible signals of  $h_{125}$ , in particular in the *golden* di-photon channel, impose *indirect* constraints on the invisible branching ratio of the discovered Higgs boson that can be substantially stronger than the *direct* constraints resulting from searches for the invisible Higgs-boson decay. Hence, for a phenomenological analysis of a model in which decays of  $h_{125}$  into hidden sectors are kinematically open it is crucial to not only consider the direct limits on  $\text{BR}_{\text{inv}}$ , but to also take into account the indirect constraints on  $\text{BR}_{\text{inv}}$  in order to not include parameter regions that are in disagreement with the experimental data from the LHC.

Secondly, we also found that the presence of a sizable value of  $\text{BR}_{\text{inv}}$  can render scenarios beyond the SM that predict modifications to the couplings of  $h_{125}$  compared to the SM viable which would otherwise be excluded by the Higgs-boson signal-rate measurements. This is trivially true in case of a universal enhancement of all Higgs-boson couplings by a common factor, where the enhancements of the couplings cancel the suppression of ordinary decay modes of  $h_{125}$  as a result of the additional decay mode  $h_{125} \rightarrow \text{inv}$ . However, also more intricate coupling modifications can be rendered viable via the presence of an invisible decay mode of  $h_{125}$ . The most striking example of our analysis is the wrong-sign Yukawa coupling regime realized in two Higgs doublet extensions of the SM with Yukawa type II and IV, which we showed to be in tension with the cross-section measurements of

$h_{125}$  assuming  $\text{BR}_{\text{inv}} = 0$ , whereas it is in very good agreement with these measurements assuming values of  $\text{BR}_{\text{inv}}$  as large as 10%.

For the variety of structures of coupling-modifiers and BSM model considered in this work, our main results are summarized in the following.

**SM-like couplings  $c_i = 1$  and  $\text{BR}_{\text{inv}} \neq 0$ .** If the Higgs boson possesses couplings to ordinary matter as predicted by the SM, we found that the invisible Higgs-boson branching ratio is constrained to be  $\text{BR}_{\text{inv}} < 6.2\%$  at 95% CL as a result of the indirect constraints from  $h_{125}$  signal-rate measurements, which is substantially smaller than the currently strongest limit  $\text{BR}_{\text{inv}} < 11\%$  resulting from the direct searches for the invisible decay of  $h_{125}$ .

**Universal couplings  $c_i = c_{\text{uni}}$  and  $\text{BR}_{\text{inv}} \neq 0$ .** We found a flat direction with  $\Delta\chi^2 = 0$  in the  $\{c_{\text{uni}}, \text{BR}_{\text{inv}}\}$  plane where the universal enhancements of the Higgs-boson couplings for  $c_{\text{uni}} > 1$  are compensated by a non-vanishing  $\text{BR}_{\text{inv}}$ . Based on the indirect constraints, universal couplings are allowed at 95% CL in the interval  $0.520 \text{BR}_{\text{inv}} + 0.960 < c_{\text{uni}} < 0.565 \text{BR}_{\text{inv}} + 1.043$ , and are ultimately only bound by the direct limit on  $\text{BR}_{\text{inv}}$ . In the case where the origin of the coupling modification is the mixing of an additional gauge-singlet scalar with the Higgs boson  $h_{125}$ , i.e.  $c_{\text{uni}} = \cos\theta$  with  $\theta$  being the mixing angle, we provided indirect limits on  $\text{BR}_{\text{inv}}$  as a function of  $\theta$  in an approximate form as given in Eq. (2.9).

**Non-universal couplings and  $\text{BR}_{\text{inv}} \neq 0$ .** We considered two examples for non-universal coupling modifications of the discovered Higgs boson. The first example consists in a common coupling modifier for the couplings to fermions, i.e.  $c_f = c_u = c_d = c_\ell$ , and a second independent coupling modifier  $c_V$  for the couplings to the gauge bosons. We found that if  $c_V \leq 1$  applies, invisible  $h_{125}$  decay modes gives rise to a decrease of the allowed ranges of both  $c_V$  and  $c_f$ . However, if also  $c_V > 1$  is considered, the  $\chi^2$  values do not generically degrade as  $\text{BR}_{\text{inv}}$  is increased to 10%. Hence, the presence of an invisible decay mode of  $h_{125}$  with sizable branching ratios opens up parameter space regions in the  $\{c_f, c_V\}$  plane that would be excluded if such a novel decay mode is not present. The second example considered is a SM-like Higgs-boson coupling to vector bosons  $c_V = 1$  but modified couplings to up and down-type quarks with the additional condition  $c_\ell = c_d$ . We found that increasing values of  $\text{BR}_{\text{inv}}$  shifts the allowed parameter space to larger values of  $c_u$  and smaller values of  $c_d = c_\ell$ , but overall yielding a degraded fit result.

**Higgs portal dark matter.** We considered dark matter candidates (scalar, fermion and vector) coupled to the Higgs boson via a single operator and computed the relic abundance and direct detection cross section in terms of the dimensionless Higgs-portal coupling parameter for each case. Direct detection experiments tightly constrain the parameter space suitable to achieve the measured relic abundance, leaving for the bosonic candidates only the mass region at the Higgs-boson resonance, i.e. if the DM mass is  $\mathcal{O}(m_{h_{125}}/2)$ . We showed that new results from the LZ collaboration rule out the fermionic DM candidate within the simplest Higgs-portal scenario under standard as-

sumptions.<sup>22</sup> Around the resonance, if we relax the hypothesis of the DM candidates to account for all the dark matter, the indirect constraints resulting from the cross-section measurements of  $h_{125}$  derived using `HiggsSignal` are the strongest bounds in the narrow range of DM masses that is not excluded by direct detection experiments.

**Singlet portal dark matter.** We studied an extension of the Higgs-portal scenario comprising an additional singlet-like scalar  $h_2$  acting as the portal between a dark matter fermion and the visible sector. As a consequence of the presence of  $h_2$ , we also took into account constraints from collider searches for additional Higgs bosons using the public code `HiggsBounds`. Firstly, we investigated a benchmark scenario in which both the decays of  $h_{125}$  into the dark-matter state and into a pair of the additional scalar are kinematically allowed, which both can contribute to  $\text{BR}_{\text{inv}}$  depending on whether  $h_2$  decays invisibly. Secondly, we investigated a benchmark scenario in which the second scalar has a mass of 80 GeV, allowing for a larger mixing between discovered Higgs boson and  $h_2$ . We identified the regions of the parameter space that are still allowed by direct detection constraints and in which part or all of the measured relic abundance of dark matter is predicted. We demonstrated that in such regions of the parameter space the indirect constraints from the cross-section measurements of  $h_{125}$  provide the strongest constraints, whereas the direct limit on  $\text{BR}_{\text{inv}}$  from searches for the invisible decay of  $h_{125}$  do not give rise to any additional constraints.

**(Pseudo) Nambu-Goldstone bosons ((P)NGB).** We considered the possibility of the Higgs boson  $h_{125}$  decaying into pairs of (P)NGBs, where the (P)NGB arises as the angular mode of a new complex scalar after the spontaneous breaking of an additional (approximate) continuous symmetry once the radial mode acquires a vev  $v_\phi$ . Using the cross-section measurements of  $h_{125}$ , we determined constraints on the mixing between  $h_{125}$  and the radial mode and on the invisible branching ratio  $\text{BR}_{\text{inv}}$ . We highlighted that if one would apply independent constraints on the mixing angle  $\theta$  and the invisible branching ratio  $\text{BR}_{\text{inv}}$ , one would consider parameter regions as allowed which are actually excluded by the cross-section measurements of  $h_{125}$ , as we showed by simultaneously taking into account both the mixing in the Higgs sector and the presence of a non-vanishing  $\text{BR}_{\text{inv}}$  in a global fit to the experimental Higgs-physics observables.

**Two Higgs doublet models.** We derived constraints in the plane  $\{\tan\beta, \cos(\alpha - \beta)\}$  for  $\tan\beta \in [0, 20]$  in the four Yukawa types of the 2HDM. We found that the  $\chi^2$ -fit result deteriorates in the type I and III as  $\text{BR}_{\text{inv}}$  is increased, leaving both types as excluded at the 95% CL for values of  $\text{BR}_{\text{inv}} > 8\%$ . On the other hand, for type II and IV a narrow region with small but positive values of  $\cos(\alpha - \beta)$  remains viable even for  $\text{BR}_{\text{inv}} = 10\%$ . We also found that in these two types the wrong-sign Yukawa coupling regime, which is barely in agreement with the measurements of  $h_{125}$  for  $\text{BR}_{\text{inv}} = 0$ , can be in very good agreement with the experimental data if the presence of an invisible decay mode of  $h_{125}$  with  $\text{BR}_{\text{inv}} > 2\%$  is assumed to be present.

---

<sup>22</sup>Given the fact that the LZ limit is close to the parameter space corresponding to the correct relic abundance, several uncertainties can affect this statement. To derive bounds on the DM nucleon scattering cross section, a local DM density of  $\rho_\odot = 0.3 \text{ GeV cm}^{-3}$  and the standard halo model for the distribution of dark matter in the Milky Way are standard assumptions from direct detection collaborations. Both quantities suffer from astrophysical uncertainties that could affect constraints from direct searches by a  $\mathcal{O}(1-3)$  factor [96]. Such uncertainties could allow the parameter space around the resonance to still be viable but on the edge of being excluded.

## Acknowledgements

The authors thank Anton Sokolov for useful discussions. The authors acknowledge support by the Deutsche Forschungsgemeinschaft (DFG, German Research Foundation) under Germany’s Excellence Strategy – EXC 2121 “Quantum Universe” – 390833306. This work has been partially funded by the Deutsche Forschungsgemeinschaft (DFG, German Research Foundation) - 491245950. This work was made possible by with the support of the Institut Pascal at Université Paris-Saclay during the Paris-Saclay Astroparticle Symposium 2021, with the support of the P2IO Laboratory of Excellence (program “Investissements d’avenir” ANR-11-IDEX-0003-01 Paris-Saclay and ANR-10-LABX-0038), the P2I axis of the Graduate School Physics of Université Paris-Saclay, as well as IJCLab, CEA, IPhT, APPEC, the IN2P3 master projet UCMN and EuCAPT ANR-11-IDEX-0003-01 Paris-Saclay and ANR-10-LABX-0038.

## A Singlet portal dark matter: additional content

### A.1 Minimization of the potential

The vevs are related to the bilinear mass parameters via the tadpole equations

$$\mu_H^2 = -\frac{1}{2} (2\lambda_H v^2 + \lambda_{\Phi H} v_\phi^2) , \quad \mu_\Phi^2 = -\frac{1}{2} (\lambda_{\Phi H} v^2 + 2\lambda_\Phi v_\phi^2) . \quad (\text{A.1})$$

Using these relations, the mass matrix of the CP-even fields  $h$  and  $\phi$  can be written as

$$\mathcal{M}^2 = \begin{pmatrix} 2\lambda_H v^2 & \lambda_{\Phi H} v v_\phi \\ \lambda_{\Phi H} v v_\phi & 2\lambda_\Phi v_\phi^2 \end{pmatrix} . \quad (\text{A.2})$$

This matrix can be diagonalized by a rotation of angle  $\theta$ , expressed in terms of the various parameters as

$$\tan(2\theta) = \frac{\lambda_{\Phi H} v v_\phi}{\lambda_\Phi v_\phi^2 - \lambda_H v^2} . \quad (\text{A.3})$$

The quartic scalar couplings are then dependent parameters that can be computed via the relations

$$\lambda_H = \frac{1}{2v^2} (m_{h_1}^2 \cos^2 \theta + m_{h_2}^2 \sin^2 \theta) , \quad (\text{A.4})$$

$$\lambda_\Phi = \frac{1}{2v_\phi^2} (m_{h_1}^2 \sin^2 \theta + m_{h_2}^2 \cos^2 \theta) , \quad (\text{A.5})$$

$$\lambda_{\Phi H} = \frac{1}{v v_\phi} (m_{h_2}^2 - m_{h_1}^2) \cos \theta \sin \theta . \quad (\text{A.6})$$

### A.2 Decay rates

The relevant partial decay width for the SM-like Higgs  $h_1 \simeq h_{125}$  are

$$\Gamma_{h_1 \rightarrow h_2 h_2} = \frac{(c_\theta^3 \lambda_{\Phi H} v + 2c_\theta^2 s_\theta v_\phi (\lambda_{\Phi H} - 3\lambda_S) + 2c_\theta s_\theta^2 v (3\lambda_H - \lambda_{\Phi H}) - \lambda_{\Phi H} s_\theta^3 v_\phi)^2}{32\pi m_{h_1}} \sqrt{1 - \frac{4m_{h_2}^2}{m_{h_1}^2}} , \quad (\text{A.7})$$

Decay rates from the physical scalars to a DM pair are given by

$$\Gamma_{h_1 \rightarrow \bar{\chi}\chi} = \frac{y_\chi^2 s_\theta^2}{8\pi} m_{h_1} \left(1 - \frac{4m_\chi^2}{m_{h_1}^2}\right)^{3/2} = \frac{s_\theta^2 m_{h_1} m_\chi^2}{8\pi v_\phi^2} \left(1 - \frac{4m_\chi^2}{m_{h_1}^2}\right)^{3/2}, \quad (\text{A.8})$$

and

$$\Gamma_{h_2 \rightarrow \bar{\chi}\chi} = \frac{y_\chi^2 c_\theta^2}{8\pi} m_{h_2} \left(1 - \frac{4m_\chi^2}{m_{h_2}^2}\right)^{3/2} = \frac{c_\theta^2 m_{h_2} m_\chi^2}{8\pi v_\phi^2} \left(1 - \frac{4m_\chi^2}{m_{h_2}^2}\right)^{3/2}. \quad (\text{A.9})$$

## References

- [1] ATLAS collaboration, *Observation of a new particle in the search for the Standard Model Higgs boson with the ATLAS detector at the LHC*, *Phys. Lett.* **B716** (2012) 1 [1207.7214].
- [2] CMS collaboration, *Observation of a new boson at a mass of 125 GeV with the CMS experiment at the LHC*, *Phys. Lett.* **B716** (2012) 30 [1207.7235].
- [3] CMS collaboration, *A portrait of the Higgs boson by the CMS experiment ten years after the discovery*, *Nature* **607** (2022) 60 [2207.00043].
- [4] ATLAS collaboration, *A detailed map of Higgs boson interactions by the ATLAS experiment ten years after the discovery*, *Nature* **607** (2022) 52 [2207.00092].
- [5] LHC HIGGS CROSS SECTION WORKING GROUP collaboration, *Handbook of LHC Higgs Cross Sections: 3. Higgs Properties*, **1307.1347**.
- [6] R.A. Lineros and M. Pierre, *Dark matter candidates in a type-II radiative neutrino mass model*, *JHEP* **21** (2020) 072 [2011.08195].
- [7] CMS collaboration, *A measurement of the Higgs boson mass in the diphoton decay channel*, *Phys. Lett. B* **805** (2020) 135425 [2002.06398].
- [8] ATLAS collaboration, *Measurement of the Higgs boson mass in the  $H \rightarrow ZZ^* \rightarrow 4\ell$  decay channel using 139 fb<sup>-1</sup> of  $\sqrt{s} = 13$  TeV pp collisions recorded by the ATLAS detector at the LHC*, **2207.00320**.
- [9] ATLAS collaboration, *Evidence for Higgs boson decays to a low-mass dilepton system and a photon in pp collisions at  $s=13$  TeV with the ATLAS detector*, *Phys. Lett. B* **819** (2021) 136412 [2103.10322].
- [10] ATLAS collaboration, *A search for the  $Z\gamma$  decay mode of the Higgs boson in pp collisions at  $\sqrt{s} = 13$  TeV with the ATLAS detector*, *Phys. Lett. B* **809** (2020) 135754 [2005.05382].
- [11] CMS collaboration, *Search for Higgs boson decays to a Z boson and a photon in proton-proton collisions at  $\sqrt{s} = 13$  TeV*, **2204.12945**.
- [12] PLANCK collaboration, *Planck 2018 results. VI. Cosmological parameters*, *Astron. Astrophys.* **641** (2020) A6 [1807.06209].
- [13] LUX collaboration, *Results from a search for dark matter in the complete LUX exposure*, *Phys. Rev. Lett.* **118** (2017) 021303 [1608.07648].
- [14] XENON collaboration, *Dark Matter Search Results from a One Ton-Year Exposure of XENON1T*, *Phys. Rev. Lett.* **121** (2018) 111302 [1805.12562].
- [15] PANDAX-4T collaboration, *Dark Matter Search Results from the PandaX-4T Commissioning Run*, *Phys. Rev. Lett.* **127** (2021) 261802 [2107.13438].
- [16] LUX-ZEPLIN collaboration, *First Dark Matter Search Results from the LUX-ZEPLIN (LZ) Experiment*, **2207.03764**.
- [17] G. Arcadi, M. Dutra, P. Ghosh, M. Lindner, Y. Mambrini, M. Pierre et al., *The waning of the WIMP? A review of models, searches, and constraints*, *Eur. Phys. J. C* **78** (2018) 203 [1703.07364].
- [18] Y. Mambrini, *Particles in the dark Universe*, no. ISBN 978-3-030-78139-2, Springer (2021).

- [19] M. Escudero, A. Berlin, D. Hooper and M.-X. Lin, *Toward (Finally!) Ruling Out Z and Higgs Mediated Dark Matter Models*, *JCAP* **12** (2016) 029 [[1609.09079](#)].
- [20] J.A. Casas, D.G. Cerdeño, J.M. Moreno and J. Quilis, *Reopening the Higgs portal for single scalar dark matter*, *JHEP* **05** (2017) 036 [[1701.08134](#)].
- [21] J. Ellis, A. Fowlie, L. Marzola and M. Raidal, *Statistical Analyses of Higgs- and Z-Portal Dark Matter Models*, *Phys. Rev. D* **97** (2018) 115014 [[1711.09912](#)].
- [22] G. Arcadi, A. Djouadi and M. Raidal, *Dark Matter through the Higgs portal*, *Phys. Rept.* **842** (2020) 1 [[1903.03616](#)].
- [23] G. Arcadi, A. Djouadi and M. Kado, *The Higgs-portal for dark matter: effective field theories versus concrete realizations*, *Eur. Phys. J. C* **81** (2021) 653 [[2101.02507](#)].
- [24] M. Cirelli, N. Fornengo and A. Strumia, *Minimal dark matter*, *Nucl. Phys. B* **753** (2006) 178 [[hep-ph/0512090](#)].
- [25] S. Bottaro, D. Buttazzo, M. Costa, R. Franceschini, P. Panci, D. Redigolo et al., *Closing the window on WIMP Dark Matter*, *Eur. Phys. J. C* **82** (2022) 31 [[2107.09688](#)].
- [26] S. Bottaro, D. Buttazzo, M. Costa, R. Franceschini, P. Panci, D. Redigolo et al., *The last complex WIMPs standing*, *Eur. Phys. J. C* **82** (2022) 992 [[2205.04486](#)].
- [27] B. Patt and F. Wilczek, *Higgs-field portal into hidden sectors*, [hep-ph/0605188](#).
- [28] A. Djouadi, A. Falkowski, Y. Mambrini and J. Quevillon, *Direct Detection of Higgs-Portal Dark Matter at the LHC*, *Eur. Phys. J. C* **73** (2013) 2455 [[1205.3169](#)].
- [29] CMS collaboration, *Search for invisible decays of the Higgs boson produced via vector boson fusion in proton-proton collisions at  $\sqrt{s} = 13$  TeV*, *Phys. Rev. D* **105** (2022) 092007 [[2201.11585](#)].
- [30] CMS collaboration, *Search for invisible decays of a Higgs boson produced through vector boson fusion in proton-proton collisions at  $\sqrt{s} = 13$  TeV*, *Phys. Lett. B* **793** (2019) 520 [[1809.05937](#)].
- [31] CMS collaboration, *Search for new physics in final states with an energetic jet or a hadronically decaying W or Z boson and transverse momentum imbalance at  $\sqrt{s} = 13$  TeV*, *Phys. Rev. D* **97** (2018) 092005 [[1712.02345](#)].
- [32] CMS collaboration, *Search for new physics in events with a leptonically decaying Z boson and a large transverse momentum imbalance in proton-proton collisions at  $\sqrt{s} = 13$  TeV*, *Eur. Phys. J. C* **78** (2018) 291 [[1711.00431](#)].
- [33] ATLAS collaboration, *Combination of searches for invisible Higgs boson decays with the ATLAS experiment*, Tech. Rep. [ATLAS-CONF-2020-052](#), CERN, Geneva (Oct, 2020).
- [34] ATLAS collaboration, *Combination of searches for invisible Higgs boson decays with the ATLAS experiment*, *Phys. Rev. Lett.* **122** (2019) 231801 [[1904.05105](#)].
- [35] ATLAS collaboration, *Search for invisible Higgs-boson decays in events with vector-boson fusion signatures using  $139 \text{ fb}^{-1}$  of proton-proton data recorded by the ATLAS experiment*, *JHEP* **08** (2022) 104 [[2202.07953](#)].
- [36] ATLAS collaboration, *Search for an invisibly decaying Higgs boson or dark matter candidates produced in association with a Z boson in pp collisions at  $\sqrt{s} = 13$  TeV with the ATLAS detector*, *Phys. Lett. B* **776** (2018) 318 [[1708.09624](#)].
- [37] ATLAS collaboration, *Search for dark matter in events with a hadronically decaying vector boson and missing transverse momentum in pp collisions at  $\sqrt{s} = 13$  TeV with the ATLAS detector*, *JHEP* **10** (2018) 180 [[1807.11471](#)].
- [38] C.E. Yaguna and O. Zapata, *Fermion and scalar two-component dark matter from a  $Z_4$  symmetry*, *Phys. Rev. D* **105** (2022) 095026 [[2112.07020](#)].
- [39] N. Okada, D. Raut and Q. Shafi, *Pseudo-Goldstone dark matter in a gauged  $B - L$  extended standard model*, *Phys. Rev. D* **103** (2021) 055024 [[2001.05910](#)].
- [40] T. Hara, S. Kanemura and T. Katayose, *Is light thermal scalar dark matter possible?*, *Phys. Rev. D* **105** (2022) 035035 [[2109.03553](#)].
- [41] J.R. Espinosa, M. Muhlleitner, C. Grojean and M. Trott, *Probing for Invisible Higgs Decays with Global Fits*, *JHEP* **09** (2012) 126 [[1205.6790](#)].

- [42] J.R. Espinosa, C. Grojean, M. Muhlleitner and M. Trott, *First Glimpses at Higgs' face*, *JHEP* **12** (2012) 045 [[1207.1717](#)].
- [43] G. Belanger, B. Dumont, U. Ellwanger, J.F. Gunion and S. Kraml, *Status of invisible Higgs decays*, *Phys. Lett. B* **723** (2013) 340 [[1302.5694](#)].
- [44] P. Bechtle, S. Heinemeyer, O. Stal, T. Stefaniak and G. Weiglein, *Probing the Standard Model with Higgs signal rates from the Tevatron, the LHC and a future ILC*, *JHEP* **11** (2014) 039 [[1403.1582](#)].
- [45] S. Kraml, T.Q. Loc, D.T. Nhung and L.D. Ninh, *Constraining new physics from Higgs measurements with Lilith: update to LHC Run 2 results*, *SciPost Phys.* **7** (2019) 052 [[1908.03952](#)].
- [46] P. Bechtle, S. Heinemeyer, T. Klingl, T. Stefaniak, G. Weiglein and J. Wittbrodt, *HiggsSignals-2: Probing new physics with precision Higgs measurements in the LHC 13 TeV era*, *Eur. Phys. J. C* **81** (2021) 145 [[2012.09197](#)].
- [47] H. Bahl, T. Biekötter, S. Heinemeyer, C. Li, S. Paasch, G. Weiglein et al., *HiggsTools: BSM scalar phenomenology with new versions of HiggsBounds and HiggsSignals*, [2210.09332](#).
- [48] G. Belanger, B. Dumont, U. Ellwanger, J.F. Gunion and S. Kraml, *Global fit to Higgs signal strengths and couplings and implications for extended Higgs sectors*, *Phys. Rev. D* **88** (2013) 075008 [[1306.2941](#)].
- [49] J. Bernon, B. Dumont and S. Kraml, *Status of Higgs couplings after run 1 of the LHC*, *Phys. Rev. D* **90** (2014) 071301 [[1409.1588](#)].
- [50] P. Bechtle, S. Heinemeyer, O. Stal, T. Stefaniak and G. Weiglein, *HiggsSignals: Confronting arbitrary Higgs sectors with measurements at the Tevatron and the LHC*, *Eur. Phys. J. C* **74** (2014) 2711 [[1305.1933](#)].
- [51] N. Berger et al., *Simplified Template Cross Sections - Stage 1.1*, [1906.02754](#).
- [52] LHC HIGGS CROSS SECTION WORKING GROUP collaboration, *Handbook of LHC Higgs Cross Sections: 1. Inclusive Observables*, [1101.0593](#).
- [53] PARTICLE DATA GROUP collaboration, *Review of Particle Physics*, *PTEP* **2020** (2020) 083C01.
- [54] ATLAS collaboration, *Analysis of  $t\bar{t}H$  and  $t\bar{t}W$  production in multilepton final states with the ATLAS detector*, Tech. Rep. [ATLAS-CONF-2019-045](#), CERN, Geneva (Oct, 2019).
- [55] ATLAS collaboration, *Measurement of Higgs boson decay into b-quarks in associated production with a top-quark pair in pp collisions at  $\sqrt{s} = 13$  TeV with the ATLAS detector*, *JHEP* **06** (2022) 097 [[2111.06712](#)].
- [56] CMS collaboration, *Measurements of Higgs boson production cross sections and couplings in the diphoton decay channel at  $\sqrt{s} = 13$  TeV*, *JHEP* **07** (2021) 027 [[2103.06956](#)].
- [57] ATLAS collaboration, *Measurement of the properties of Higgs boson production at  $\sqrt{s}=13$  TeV in the  $H \rightarrow \gamma\gamma$  channel using  $139 \text{ fb}^{-1}$  of pp collision data with the ATLAS experiment*, [ATLAS-CONF-2020-026](#) (2020) .
- [58] M. Cepeda et al., *Report from Working Group 2: Higgs Physics at the HL-LHC and HE-LHC*, *CERN Yellow Rep. Monogr.* **7** (2019) 221 [[1902.00134](#)].
- [59] ATLAS, CMS collaboration, *Measurements of the Higgs boson production and decay rates and constraints on its couplings from a combined ATLAS and CMS analysis of the LHC pp collision data at  $\sqrt{s} = 7$  and 8 TeV*, *JHEP* **08** (2016) 045 [[1606.02266](#)].
- [60] CMS collaboration, *Combined measurements of Higgs boson couplings in proton–proton collisions at  $\sqrt{s} = 13$  TeV*, *Eur. Phys. J. C* **79** (2019) 421 [[1809.10733](#)].
- [61] ATLAS collaboration, *Combined measurements of Higgs boson production and decay using up to  $80 \text{ fb}^{-1}$  of proton-proton collision data at  $\sqrt{s} = 13$  TeV collected with the ATLAS experiment*, *Phys. Rev. D* **101** (2020) 012002 [[1909.02845](#)].
- [62] P. Fileviez Perez, H.H. Patel, M.J. Ramsey-Musolf and K. Wang, *Triplet Scalars and Dark Matter at the LHC*, *Phys. Rev. D* **79** (2009) 055024 [[0811.3957](#)].
- [63] J.M. No, *Looking through the pseudoscalar portal into dark matter: Novel mono-Higgs and mono-Z signatures at the LHC*, *Phys. Rev. D* **93** (2016) 031701 [[1509.01110](#)].
- [64] C. Arina, A. Beniwal, C. Degrande, J. Heisig and A. Scaffidi, *Global fit of pseudo-Nambu-Goldstone Dark Matter*, *JHEP* **04** (2020) 015 [[1912.04008](#)].

- [65] T. Biekötter and M.O. Olea-Romacho, *Reconciling Higgs physics and pseudo-Nambu-Goldstone dark matter in the S2HDM using a genetic algorithm*, *JHEP* **10** (2021) 215 [2108.10864].
- [66] CMS collaboration, *Analysis of the CP structure of the Yukawa coupling between the Higgs boson and  $\tau$  leptons in proton-proton collisions at  $\sqrt{s} = 13$  TeV*, *JHEP* **06** (2022) 012 [2110.04836].
- [67] J.A. Aguilar-Saavedra, D.E. López-Fogliani, C. Muñoz and M. Pierre, *WIMP dark matter in the  $U\mu\nu$ SSM*, *JCAP* **05** (2022) 004 [2111.07091].
- [68] J.M. Cline, K. Kainulainen, P. Scott and C. Weniger, *Update on scalar singlet dark matter*, *Phys. Rev. D* **88** (2013) 055025 [1306.4710].
- [69] O. Lebedev, H.M. Lee and Y. Mambrini, *Vector Higgs-portal dark matter and the invisible Higgs*, *Phys. Lett. B* **707** (2012) 570 [1111.4482].
- [70] DARWIN collaboration, *DARWIN: towards the ultimate dark matter detector*, *JCAP* **1611** (2016) 017 [1606.07001].
- [71] J. Billard, L. Strigari and E. Figueroa-Feliciano, *Implication of neutrino backgrounds on the reach of next generation dark matter direct detection experiments*, *Phys. Rev. D* **89** (2014) 023524 [1307.5458].
- [72] M. Cirelli, E. Del Nobile and P. Panci, *Tools for model-independent bounds in direct dark matter searches*, *JCAP* **1310** (2013) 019 [1307.5955].
- [73] A. Alloul, N.D. Christensen, C. Degrande, C. Duhr and B. Fuks, *FeynRules 2.0 - A complete toolbox for tree-level phenomenology*, *Comput. Phys. Commun.* **185** (2014) 2250 [1310.1921].
- [74] G. Bélanger, F. Boudjema, A. Goudelis, A. Pukhov and B. Zaldivar, *micrOMEGAs5.0 : Freeze-in*, *Comput. Phys. Commun.* **231** (2018) 173 [1801.03509].
- [75] G. Belanger, F. Boudjema, A. Pukhov and A. Semenov, *micrOMEGAs-3: A program for calculating dark matter observables*, *Comput. Phys. Commun.* **185** (2014) 960 [1305.0237].
- [76] A. Freitas, S. Westhoff and J. Zupan, *Integrating in the Higgs Portal to Fermion Dark Matter*, *JHEP* **09** (2015) 015 [1506.04149].
- [77] P. Bechtle, O. Brein, S. Heinemeyer, G. Weiglein and K.E. Williams, *HiggsBounds: Confronting Arbitrary Higgs Sectors with Exclusion Bounds from LEP and the Tevatron*, *Comput. Phys. Commun.* **181** (2010) 138 [0811.4169].
- [78] P. Bechtle, O. Brein, S. Heinemeyer, G. Weiglein and K.E. Williams, *HiggsBounds 2.0.0: Confronting Neutral and Charged Higgs Sector Predictions with Exclusion Bounds from LEP and the Tevatron*, *Comput. Phys. Commun.* **182** (2011) 2605 [1102.1898].
- [79] P. Bechtle, O. Brein, S. Heinemeyer, O. Stal, T. Stefaniak, G. Weiglein et al., *HiggsBounds – 4: Improved Tests of Extended Higgs Sectors against Exclusion Bounds from LEP, the Tevatron and the LHC*, *Eur. Phys. J. C* **74** (2014) 2693 [1311.0055].
- [80] P. Bechtle, D. Dercks, S. Heinemeyer, T. Klingl, T. Stefaniak, G. Weiglein et al., *HiggsBounds-5: Testing Higgs Sectors in the LHC 13 TeV Era*, *Eur. Phys. J. C* **80** (2020) 1211 [2006.06007].
- [81] ATLAS collaboration, *Search for Higgs boson decays into a pair of pseudoscalar particles in the  $b\bar{b}\mu\mu$  final state with the ATLAS detector in pp collisions at  $\sqrt{s}=13$  TeV*, *Phys. Rev. D* **105** (2022) 012006 [2110.00313].
- [82] OPAL collaboration, *Search for invisibly decaying Higgs bosons in  $e^+ e^- \rightarrow Z0 h0$  production at  $s^{**}(1/2) = 183\text{-GeV} - 209\text{-GeV}$* , *Phys. Lett. B* **682** (2010) 381 [0707.0373].
- [83] LEP WORKING GROUP FOR HIGGS BOSON SEARCHES, ALEPH, DELPHI, L3, OPAL collaboration, *Search for the standard model Higgs boson at LEP*, *Phys. Lett. B* **565** (2003) 61 [hep-ex/0306033].
- [84] L3 collaboration, *Search for an invisibly-decaying Higgs boson at LEP*, *Phys. Lett. B* **609** (2005) 35 [hep-ex/0501033].
- [85] S. Weinberg, *Goldstone Bosons as Fractional Cosmic Neutrinos*, *Phys. Rev. Lett.* **110** (2013) 241301 [1305.1971].



- [86] E. Fernandez-Martinez, M. Pierre, E. Pinsard and S. Rosauero-Alcaraz, *Inverse Seesaw, dark matter and the Hubble tension*, *Eur. Phys. J. C* **81** (2021) 954 [[2106.05298](#)].
- [87] S. Dawson and M. Sullivan, *Enhanced di-Higgs boson production in the complex Higgs singlet model*, *Phys. Rev. D* **97** (2018) 015022 [[1711.06683](#)].
- [88] T.D. Lee, *A Theory of Spontaneous T Violation*, *Phys. Rev. D* **8** (1973) 1226.
- [89] J.E. Kim, *Weak Interaction Singlet and Strong CP Invariance*, *Phys. Rev. Lett.* **43** (1979) 103.
- [90] G.C. Branco, P.M. Ferreira, L. Lavoura, M.N. Rebelo, M. Sher and J.P. Silva, *Theory and phenomenology of two-Higgs-doublet models*, *Phys. Rept.* **516** (2012) 1 [[1106.0034](#)].
- [91] B. Grzadkowski and P. Osland, *Tempered Two-Higgs-Doublet Model*, *Phys. Rev. D* **82** (2010) 125026 [[0910.4068](#)].
- [92] T. Biekötter, P. Gabriel, M.O. Olea-Romacho and R. Santos, *Direct detection of pseudo-Nambu-Goldstone dark matter in a two Higgs doublet plus singlet extension of the SM*, *JHEP* **10** (2022) 126 [[2207.04973](#)].
- [93] M. Bauer, U. Haisch and F. Kahlhoefer, *Simplified dark matter models with two Higgs doublets: I. Pseudoscalar mediators*, *JHEP* **05** (2017) 138 [[1701.07427](#)].
- [94] A. Falkowski, F. Riva and A. Urbano, *Higgs at last*, *JHEP* **11** (2013) 111 [[1303.1812](#)].
- [95] P.M. Ferreira, J.F. Gunion, H.E. Haber and R. Santos, *Probing wrong-sign Yukawa couplings at the LHC and a future linear collider*, *Phys. Rev. D* **89** (2014) 115003 [[1403.4736](#)].
- [96] P.F. de Salas and A. Widmark, *Dark matter local density determination: recent observations and future prospects*, *Rept. Prog. Phys.* **84** (2021) 104901 [[2012.11477](#)].